Univerzita Karlova
Přírodovědecká fakulta

Studijní program: Biologie

Obor: Fyziologie živočichů

Bc. Gabriela Šejnová

Vliv stochastického chování iontových kanálů na přenos signálu a informace na excitabilních neuronálních membránách

The influence of stochastic behaviour of ion channels on the signal and information transfer at excitable neuronal membranes

Diplomová práce

Vedoucí diplomové práce: Mudr. Eduard Kuriščák, Ph.D.

Praha 2017

Prohlášení

Prohlašuji, že jsem závěrečnou práci zpracoval/a samostatně a že jsem uvedl/a všechny použité informační zdroje a literaturu. Tato práce ani její podstatná část nebyla předložena k získání jiného nebo stejného akademického titulu.

V Praze,

Podpis

Acknowledgement

I would like to express my gratitude to my supervisor Mudr. Eduard Kuriščák, Ph.D. for all the useful remarks and comments and also for his invested time and patience during the elaboration of this thesis.

I also thank to my family and closest ones for their support throughout my studies.

Abstract

The stochastic behavior of voltage-gated ion channels causes fluctuations of conductances and voltages across neuronal membranes, contributing to the neuronal noise which is ubiquitous in the nervous system. While this phenomenon can be observed also on other parts of the neuron, here we concentrated on the axon and the way the channel noise influences axonal input-output characteristics. This was analysed by working with our newly created computational compartmental model, programmed in Matlab environment, built up using the Hodgkin-Huxley mathematical formalism and channel noise implemented via extended Markov Chain Monte Carlo method. The model was thoroughly verified to simulate plausibly a mammalian axon of CA3 neuron.

Based on our simulations, we confirmed quantitatively the findings that the channel noise is the most prominent on membranes with smaller number of Na^+ and K^+ channels and that it majorly increases the variability of travel times of action potentials (APs) along axons, decreasing thereby the temporal precision of APs. The simulations analysing the effect of axonal demyelination and axonal diameter correlated well with other finding referred in Literature. We further focused on spike pattern and how is its propagation influenced by inter-spike intervals (ISI). We found, that APs fired within intervals as short as 2 ms have slowest propagation speeds compared to those that occur alone or separated by large time intervals. This effect was partially reduced by increasing the stimulation amplitudes triggering individual APs. Channel noise showed similar effect rectifying the alteration of speed propagation caused by varying ISI. Our simulations demonstrate deteriorating as well as non-deteriorating effects of channel noise dominated by nonlinear behavior of voltage-gated channel. Our further examinations will aim on elaborating this idea in the frame of stochastic resonance, known to be providing some signal benefits in strongly nonlinear and noisy systems.

Keywords: ion channels, stochastic modelling, signal transfer, Markov chains, axons, neuronal membrane, action potential

Abstrakt

Stochastické chování napěťově řízených iontových kanálů způsobuje fluktuace v konduktanci a napětí na neuronálních membránách, čímž přispívá k všudypřítomnému šumu v nervové soustavě. Přestože se tento fenomén vyskytuje i na jiných částech neuronu, zde jsme se soustředili pouze na axon a na způsob, jakým neuronální šum ovlivňuje axonální vstupně-výstupní charakteristiky. Problematika byla analyzována za použití nového výpočetního kompartmentálního modelu, který jsme naprogramovali v prostředí Matlab, a který je založený na matematickém Hodgkin-Huxley formalismu s kanálovým šumem implementovaným pomocí rozšířené metody Markovových řetězců Monte Carlo. Model byl důkladně ověřen k tomu, aby věrně simuloval savčí axon CA3 neuronu.

Na základě našich simulací jsme kvantitativně potvrdili dosavadní poznatek, že neuronální šum je výraznější na membránách s nižším počtem Na^+ a K^+ kanálů, a že výrazně zvyšuje variabilitu doby propagace akčního potenciálu (AP) podél axonu, čímž i snižuje časovou preciznost AP. Simulace analyzující efekt demyelinizace axonu a axonálního průměru korelovala s dřívějšími poznatky zmíněnými v Literatuře. Dále jsme se soustředili na vzorce akčních potenciálů a jak je jejich propagace ovlivněna intervaly mezi nimi (ISI, inter-spike intervals). Zjistili jsme, že AP vypálené s krátkými intervaly 2 ms mají nejpomalejší propagační rychlost v porovnání s těmi, které se vyskytují samy nebo oddělené dlouhými intervaly. Tento efekt byl částečně snížen zvyšováním stimulační amplitudy pro jednotlivé AP. Kanálový šum prokazoval podobný efekt usměrňování změn rychlosti propagace v důsledku proměnlivých ISI. Naše simulace demonstrují deteriorační i nedeteriorační efekty kanálového šumu ovládané nelineárním chováním napěťově řízených kanálů. Náš budoucí výzkum bude zaměřen na rozvedení této myšlenky v rámci stochastické rezonance, známé svými výhodami z hlediska signálu v silně neilineárních systémech s výrazným šumem.

Klíčová slova: iontové kanály, stochastické modelování, přenos signálu, Markovovy řetězce, axon, neuronální membrána, akční potenciál

Contents

Abbreviations

AP	Action potential
CA3	Region 3 of the Ammon's horn in hippocampus
CNS	Central nervous system
EPSC	Excitatory postsynaptic currents
EPSP	Excitatory postsynaptic potential
G-ratio	Ratio of the inner axon diameter to the total outer diameter
HCN	Hyperpolarization-activated cyclic nucleotide–gated (channels)
H-H	Hodgkin-Huxley
ISI	Interspike intervals
K_v	Voltage-gated potassium channels
MCMC	Markov Chain Monte Carlo
Na_v	Voltage-gated sodium channels
SD	Standard deviation
SDE	Stochastic differential equations

1 Introduction

The voltage-gated ion channels are an essential part of cellular membranes, especially in neurons where they enable the flow of current across the membrane and thus are responsible for action potential generation and its transfer between neurons. Their kinetics were first mathematically described by Hodgkin and Huxley (Hodgkin et al. 1951), who performed a set of experiments on the giant squid axon and formulated a *set of differential equations*. These have eversince served as a reliable representation of the changes of current and membrane potential on axons during the propagation of action potentials.

However, this model is based on the assumption that such behaviour is purely deterministic, which has shown to be incorrect. The voltage-gated ion channels (the subject of our interest are the *sodium*, Na^+ and *potassium*, K^+ *channels*) have multiple independent subunits which close and open randomly, switching between multiple conformations. This causes small fluctuations of the membrane potential (tens of microvolts), called as the *ion channel noise*. It has been assumed that this noise has a negative impact on the signal transfer as it decreases its precision of propagation and might participate on cognitive decline during aging or neurodegenerative diseases (Welford 1965; Kail 1997). However, more possible effects of the voltage-gated channel noise have been found over the past decades, and its precise function in the CNS is still unclear.

The neuronal noise can be studied either experimentally (mainly using the patch clamp technique) or via computational models. We have chosen the latter method as it provides more options to observe the influence of noise on various axonal characteristics. Our goal was to create a detailed, biologically precise computational model of a mammalian axon and to study the various attributes of noise depending on different parameter configurations.

2 Literature review

The brain is a complex structure consisting of a vast number of neurons (86,000,000,000 in humans) mutually connected with synapses. We can observe various functional structures on both intracellular and intercellular levels as well as on the scale of neuronal networks. However, the main function of our nervous system is in the processing of information and its transfer. The base unit of this process is the neuron and the action potentials (AP) it can generate and propagate. The molecular mechanisms behind it are well known, yet the precise function of neuronal spikes in information coding remains to be clarified. One way to look at this matter is from the biophysical perspective – by analysing the input-output characteristics of neurons and their compartments. Each of the individual information channels – such as the dendritic spine, dendritic tree, neuronal soma, the axon and its branching – can contribute to our overall image of the mechanisms underlying information coding and processing.

The research part of this work is aimed at the input-output characteristics of the axon, therefore the further review will be focused mainly on this part of the neuron.

2.1 Signal transfer in axons

2.1.1 Passive membrane properties

The core element responsible for the majority of biophysical properties in neurons is the cell membrane. An important property of this lipid bilayer is that it can separate charges and create an electrochemical potential of approx. -70 mV. Excitation of such membrane above certain threshold can lead to action potential generation and its conduction along the nerve cable is then responsible for the propagation of the spike (Ehrenstein & Lecar 1972).

The nature of any electrical potential is a separation of charge – this is a principle of the capacitor, consisting of two conducting plates or solutions with an insulating layer between them. The amount of charge needed to be transferred between two conductors to create a change in the potential is called capacitance, C. The current flowing into

an ideal capacitor can then reversibly transfer the charge from one coductor to another. In neurons we can describe the relationship between capacitance, electric potential and current using a simple differential equation (1) which allows us to observe how these characteristics change in time (Hille 2001).

$$C\frac{dV_m(t)}{dt} + \frac{V_m(t) - V_{rest}}{R} = I_{inj}(t) \quad (1)$$

C is for the capacitance of membrane patch, V_m is the membrane potential, V_{rest} the membrane resting potential, $I_{inj}(t)$ the current flow across the membrane, R membrane resistance and t for time.

If we consider the signal propagation along the axon to be a passive process (which can be plausible at longer distances), the energy needed for the preservation of information is taken from the electrochemical gradient and its dynamics is summarised in the equation called the *cable theory* (2). In such model the axon is represented as a series of interconnected cylinders, where the membrane resistance, r_m, is related to the cylinder surface and the longitudinal resistance located along the cylinder is the axoplasmic resistance r_a. The average resistance given by the flow of current both along the axon and across the membrane is called the input resistance, $r_{input,}$ and defines potential change V_0 (Nicholls et al. 2012).

Another useful parameter used in the cable description is the length constant. If we apply electric potential using a microelectrode at a certain place along the passive cable, this potential will spread along the fibre in both ways with exponential decrease. The length constant λ is the distance at which the potential drops to 1/e (37 %) of its initial value. Higher value of r_m decreases loss of current across the membrane and thus increases the length constant (i.e. the distance at which the potential change can spread). On the contrary, r_a restrains the longitudinal flow of current and thus decreases λ. Furthermore, the length constant as well as r_{input} are also dependent on the axonal diameter – the input resistance decreases with a 3/2 root of the fibre radius, whereas λ increases with the radius square root (Nicholls et al. 2012).

$$\lambda^2 \frac{\partial^2 V_m(x,t)}{\partial x^2} = \tau_m \frac{\partial V_m(x,t)}{\partial t} + (V_m(x,t) - V_{rest}) - r_m I_{inj}(x,t) \quad (2)$$

$\lambda=\sqrt{(r_m/r_a)}$ is the length constant; $(r_m=R_m/\pi_d)$ is the membrane resistance of cable unit lenght, $R_m=R \cdot S$ is a specific membrane resistance, S is membrane surface and d is cable diameter. $r_a=4R_i/\pi d$ is for the intracellular resistance of the cable unit length (R_i = intracellular resistivity), τ_m is membrane time constant ($c_m=C_m \cdot \pi d$ is membrane capacitance of cable unit length, C_m=C/S for specific membrane capacitance). $V_m(x,t)$ is the cable voltage in the position x at time t (Kuriscak 2002).

The neuronal membrane has a capacitance around 1 μF/cm2, which is a relatively high number and thus requires a certain minimal amount of ions to flow at a sufficient speed to generate the desired - electrical impulse. As a consequence, the voltage response to any current input is slowed down by a specific time τ, which is called the time constant. It depends on the membrane resistance and capacitance (3) and has an exponential course (Hille 2001).

$$\tau = Rm \times Cm \quad (3)$$

τ is time constant, R_m membrane resistance and C_m membrane capacitance.

The time constant in neural cells varies between 1 – 20 ms and it is by definition the time needed for the increase of potential up to 63 % of its final value. This is however valid only for simple spherical cell, the axonal membrane is more specific in this matter. At a certain point the current stops charging the capacitor and different parts of the cable RC circuits interact with each other. Therefore, the function is not exponential anymore and the rise and fall of potential changes elongates with the distance between the pulse application and its detection (see *Fig. 1*.) (Sperelakis 2012).

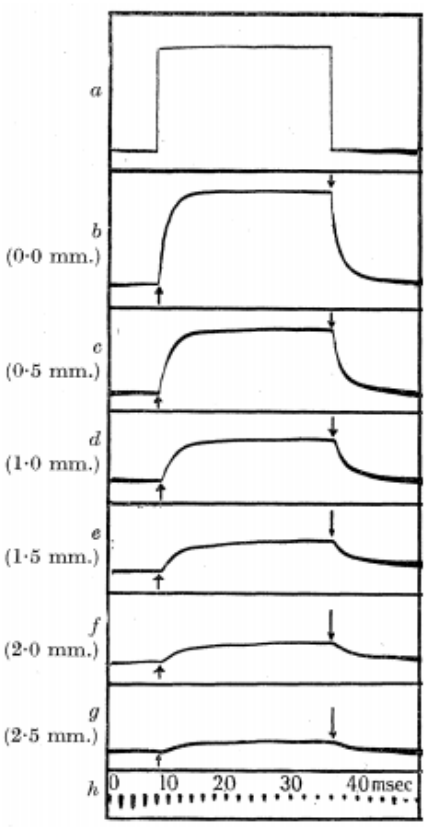

Fig. 1. Cable theory. Passive propagation of signals along axon. A rectangular pulse was injected in the axon of Homarus (a) and the propagation of changes in potential was recorded at different distances from the cathode (listed in brackets). The longer the distance, the milder is the increase and decrease of the potential change (Adapted from Hodgkin & Rushton, 1946).

2.1.2 The spread of action potentials

All the characteristics described so far are connected with the passive signal propagation, of which the gradual decay is approaching linear behaviour. It is now necessary to also mention the nonlinear membrane properties together with their typical example – action potentials.

Action potentials are usually initiated at the beginning of the axon (in the specific part called the *axon hillock*) and are propagated towards the end. If we inject current in the middle of tha axonal fibre, the potential changes spread equally in both ways. However, at any given place on the membrane the AP cannot occur more than once in a short period of time because of the so called *refractory period* – a temporarily decreased conductance of sodium channels due to the channel inactivation. Before another excitation or inhibition can occur on the membrane, this inactivation must subside (Nicholls et al. 2012; Sperelakis 2012).

In the invertebrate, most axons are left uncovered and have an even distribution of ion channels. The spike propagation is therefore more continuous and neither the conductances, nor membrane or axoplasmic resistances change along the fibre. On the contrary, the vertebrates have most of their axons wrapped in multiple (dozens to hundreds) layers of the lipid myelin. Myelination has not only a protective function, but it also insulates the axon and thus increases the transverse resistance and decreases the membrane capacitance (Tasaki 1955). The isolation is so strong that almost no ions can travel across the membrane and the action potentials can only be generated in short unmyelinated sections called *the nodes of Ranvier*. Such compartments are approximately 1 – 2 μm long and the internodes between them can vary in length between hundreds of μm up to several milimeters. The distribution of ion channels is variable in myelinated axons – sodium channels are located mainly in the Ranvier nodes and in far lesser density in the internodes, whereas the concentration of potassium channels is distributed *vice versa* (Nicholls et al. 2012). Due to the mentioned properties, the propagation of action potential in myelinated axons has the character of *saltatory conduction* – the signal travels along the myelinated parts "unobserved" and the spikes occur only at the Ranvier nodes, which creates the impression as if they were "jumping" (Huxley & Stämpeli 1949).

Now that we have described the basic principles of how potential changes are trasmitted in axons, it is important to look more closely on the submolecular level – namely on the ion channels and the way they are involved in action potential generation.

2.2 Voltage-gated ion channels

2.2.1 Electrophysiology of gating

When the cell is in a quiescent state, there is a relatively constant intracellular and extracellular concentration of specific ions. In neurons, there are multiple factors responsible for maintaining such balance (for example the potassium ions tend to "escape" the cell through permeable ion channels. Moreover, its interstitial concentrations can be modified by astrocytes. The most important regulator is the Na^+/K^+-ATPase, a membrane pump which transports two potassium ions inside the cell

in exchange for three sodium ions transported outside, against their concentration gradient. This pump helps to restore the original ion concentrations and to maintain the *resting potential* - a relatively stable membrane voltage of in the range between -20 and -90 mV (-70 mV for neurons, -80 to -90 mV for the astroglia, -40 mV for photoreceptor cells (Tortora & Derrickson 2008)). Mainly the sodium, potassium and chloride ions play their roles in the resting state and their contribution is described in the Goldman-Hodgkin-Katz voltage equation (4) (Sperelakis 2012).

$$E_m = \frac{RT}{F} \times ln\left(\frac{P_{Na+}[Na^+]_o + P_{K+}[K^+]_o + P_{Cl-}[Cl^-]_i}{P_{Na+}[Na^+]_i + P_{K+}[K^+]_i + P_{Cl-}[Cl^-]_o}\right) \quad (4)$$

Hodgkin-Katz equation. Em is the resting potential, T temperature, F is Faraday constant, R ideal gas constant, [ion]out/in is extracellular or intracellular concentration of given ion and P is the relative permeability.

When the cell receives a stimulus, the voltage at the membrane is temporarily changed. This is possible because of ion channels, which open only under certain conditions. Opening of such channels can be achieved for example by binding of a specific ligand (ligand-gated channels) or a second messenger, while some channels are voltage-sensitive and thus react to depolarization or repolarization of the membrane. This last group – especially the sodium and potassium channels - is very important in the generation of conducted signals in neurons. These channels can switch among the following gating states: activated, inactivated and the resting state. Both the inactivated and the resting state are non-conducting – the difference between them is that the inactivated state is refractory due to a prolonged depolarisation and once it becomes repolarised, it can return to the resting phase (Catterall 1995). Another important point is that ion channel, at given instant, is always either open or closed, there are no transitional stages inbetween (Hille 2001).

When the channel is open, the ions can flow inside or outside the cell along their concentration gradient. If the membrane potential is such that the particular ion type stops flowing through the membrane, we speak about the *equilibrium potential.* In a single-ion system it can be also called *reversal* or the *Nernst potential,* and the exact value can be calculated using the *Nernst equation* (5). This state is like passive or static equilibrium, in contrast with the resting potential, which is in a dynamic equlibrium and a high energy expenditure for ionic pumps (Nicholls et al. 2012).

$$E = \frac{RT}{zF} \times \ln \frac{[ion]_{out}}{[ion]_{in}} \quad (5)$$

Nernst equation. E is the Nernst potential, z is ion charge, T temperature, F is Faraday constant, R ideal gas constant, $[ion]_{out}$ is extracellular ion concentration and $[ion]_{in}$ intracellular ion concentration.

The ions flow through the open channel with a specific *driving force*, which is given by the difference between the actual membrane potential and the reversal potential (6). This value tells us how far an ion is from its equilibrium and the arithmetic sign can help us predict the direction of ion flux (Bezanilla 2005).

$$i = \gamma(V - E) \quad (6)$$

i is ion current flow, γ is the channel conductance, V applied voltage and E reversal potential (Bezanilla 2005).

2.2.2 Biological structure

The gating properties of individual channel types depend on their structure, which can be variable. Here we concentrate on the typical mammalian ion channels located in the axons. The most common sodium (Na_v) channels have one α subunit – a long polypeptide with four domains, whereas the potassium channels (K_v) have four α-subunits, each with a single domain. All these domains have six α-helical transmembrane segments (labelled S1 - S6). The first four can be either identical or variable, whereas S5 and S6 together with the pore loop are forming the gate and thus enabling ion conduction. The fourth segment is rich in arginines and has a voltage-sensing function (Lai & Jan 2006).

Additionally, the sodium channels have also incorporated one or more β subunits. So far there have been identified five different mammalian Na_v β subunits: β1, β1B (an alternative splice variant of β1), β2, β3 and β4. Numerous studies have convincingly demonstrated their role in regulation of gating and kinetics of the α subunits (Isom et al. 1992; Isom et al. 1995; Kazen-Gillespie et al. 2000; Morgan et al. 2000; Qin et al. 2003; Yu et al. 2003). However, further functions of these proteins have emerged in the past years. For example, deletion of β1 in mice leads to ataxia, reduction of mature Ranvier nodes in the optic nerve, partial absence of paranodal septate-like junctions adjacent to these nodes and reduced density of Na_v 1.1 channels in a subset of pyramidal neurons

in the CA2/CA3 region. This suggests that β1 subunits are not only required for normal conduction of action potentials, but can also influence sodium channel density and localization and play a role in the axo-glial communication at nodes of Ranvier (Yu et al. 2003). The extracellular domains of these subunits have an immunoglobulin-like structure and are also involved in multiple cell adhesion-related activities (Malhotra et al. 2000; Yu et al. 2003). Altogether, it is now evident that the β subunits have a multifunctional character and are not mere auxiliary segments of Na_v channels, as was supposed in the past.

The voltage-gated potassium channels have certain structural specifics as well. There are multiple families of these proteins, yet the most important ones for the purpose of our research are those located on the axon – the Kv1 and Kv7 (KCNQ) channels. Kv1 have been shown to reduce axonal excitability and to regulate the release of neurotransmitters into the synaptic cleft in the CA3 neurons (Debanne et al. 1997; Smart et al. 1998). In this group, the tetramerization of α subunits is initiated by the N-terminal T1 domain, which also probably mediates the interaction of the Kvβ1 and Kvβ2 subunits with the most frequent α subunits located in the CNS (Gulbis et al. 2000; Pongs et al. 1999; Rhodes et al. 1997). The Kv7 family is activated at sub-threshold levels and acts as a delayed rectifier. This was demonstrated by application of Retigabine, which opens KCNQ channels and reduces axonal excitability. Furthermore, the KCNQ blocker Linopirdine prolonges the duration of repolarization in neonatal nerves and mutations in the gene encoding KCNQ2 lead to neonatal epilepsy and myokymia (Devaux 2004).

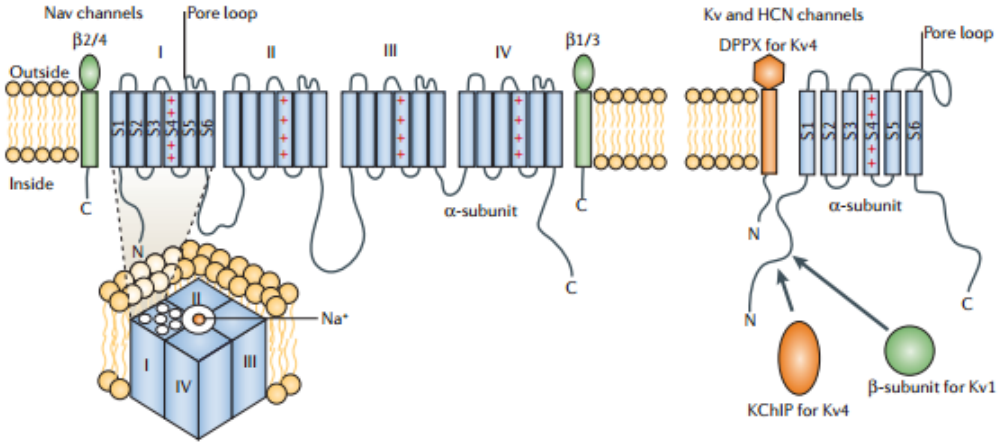

Fig. 2. Typical structure of voltage-gated sodium channels. A single polypeptide is formed of four domains (*I-IV*), each consisting of 6 transmembrane segments (*S1-S6*). The β subunits ($\beta_{1/3}$ and $\beta_{2/4}$) have an extracellular domain with Ig-like structure, which interacts with α subunits and is also involved in cell adhesion. Both the voltage-gated potassium channels (*Kv*) and cyclic-nucleotide-gated (*HCN*) channels have four α subunits. Kv1 channels have in addition the cytoplasmatic β subunits, whereas Kv4 are associated with KChIP intracellular protein and with a single-span membrane protein DPPX (adapted from Lai & Jan, 2006).

In summary, the different subunit composition in each channel type enables them to react differently towards electrical or chemical changes and thus help to adjust the threshold, frequency or shape of spikes and overall excitability of individual neurons. While the Na_v channels are involved in the membrane depolarization and the rising phase of action potentials, the K_v channels repolarize or hyperpolarize the membrane and thus can vary the intervals between spikes and change, along with other channels, the sensitivity of neurons to the synaptic input.

2.3 Hodgkin-Huxley equations

The dependence of ion channel conductance on the voltage changes was first quantitatively formalized by Hodgkin and Huxley (A. L. Hodgkin & Huxley 1952). They measured the current flow through a membrane of a giant squid nerve fibre and, based on their observations, derived a set of deterministic nonlinear differential equations (Hodgkin et al. 1949; Hodgkin et al. 1951). They took into account only the sodium and potassium channels, as these have the main impact, and summed the rest of ion channels into the leakage current. While the sodium and potassium conductances (g_{Na} and g_K)

depend on the voltage changes, the leakage current g_L does not. The sum of these three ionic currents (sodium, potassium and leakage) together with the lipid bilayer current is then taken as the total current I (7).

$$I = C_m \frac{dV_m}{dt} + I_K + I_{Na} + I_L \quad (7)$$

I is the total membrane current per unit area, C_m is the membrane capacitance per unit area, V_m the membrane potential, t time and I_K, I_{Na} and I_L are the ion channel currents.

Because all of the individual ion channels switch stochastically between closed and open states, both sodium and potassium ionic current conductances are multiplied by the fraction of channels which are currently open. However, each ion channel type has different dynamics and thus is described by different equation.

2.3.1 Dynamics of potassium ion channels

Typically, the voltage-gated potassium channels have four independent gates and all of them need to be open so that the channel is conducting. Each of the gates is open with the probability n, which is a value between 0 and 1. Then the probability that all four gates are open is n^4 and is multiplied by the maximal channel conductance g_k (with the value of 36 mS/cm^2 for squid axon (Alan L. Hodgkin & Huxley 1952)) to depict the actual conductance of the potassium channels (8).

$$I_K = \bar{g}_K n^4 (V - V_K) \quad (8)$$

I_K is the potassium channel current, V_K is the reversal potential of potassium channels and V is the applied membrane voltage.

If the probability that a gate is open is n, then the probability for it being closed is 1-n. The transition between these states is following:

$$\text{n} \underset{\alpha_n}{\overset{\beta_n}{\rightleftharpoons}} \text{1-n}$$

where α_n is the transition rate from the closed to the open state, and β_n is the transition rate from the open state to closed. These rates are voltage dependent

and their units are 1/ms. Then the change of probability of the channel being open can be described by the first-order linear differential equation (9).

$$\frac{dn}{dt} = \propto_n (V)(1-n) - \beta_n(V)n \tag{9}$$

Hodgkin and Huxley assigned the opening and closing rates of potassium channels as (A. L. Hodgkin & Huxley 1952)

$$\propto_n (V) = \frac{0.01(V+10)}{exp\left(\frac{V+10}{10}\right)-1} \tag{10}$$

and

$$\beta_n = 0.125\ exp\left(\frac{V}{80}\right) \tag{11}$$

where V is in millivolts (mV).

2.3.2 Dynamics of sodium ion channels

The sodium channel dynamics of H-H model is more complicated as the channel is open when all three sites are occupied by their activating molecule and are not blocked by an inactivating protein. Hodgkin and Huxley therefore distinguished an activating gate *m* and inactivating gate *h.* The sodium ion current I_{Na} is then given by

$$I_{Na} = \bar{g}_{Na} m^3 h (V - V_{Na}) \tag{12}$$

where g_{Na} is the maximum sodium conductance (120 mS/cm^2 in squid axon (Alan L. Hodgkin & Huxley 1952)), V_{Na} the sodium reversal potential and V is the applied voltage (A. L. Hodgkin & Huxley 1952).

Here m^3 represents the proportion of the present activating molecules and *1-m* represents the proportion of their absence. Similarly, h is the probability that the inactivating molecule is absent and *1-h* is the probability that it is there. The equations for *m* and *h* are the same as for *n*:

$$\frac{dm}{dt} = \propto_m (V)(1-m) - \beta_m(V)m \tag{13}$$

and

$$\frac{dh}{dt} = \propto_h (V)(1-h) - \beta_h(V)h \tag{14}$$

The transition rates α_m, β_m, α_h and β_h were formulated as:

$$\propto_m (V) = \frac{0.1(V+25)}{exp\left(\frac{V+25}{10}\right)-1} \tag{15}$$

$$\beta_m(V) = 4\ exp\left(\frac{V}{18}\right) \tag{16}$$

$$\propto_h (V) = 0.07\ exp\left(\frac{V}{20}\right) \tag{17}$$

$$\beta_h(V) = \frac{1}{exp\left(\frac{V+30}{10}\right)+1} \tag{18}$$

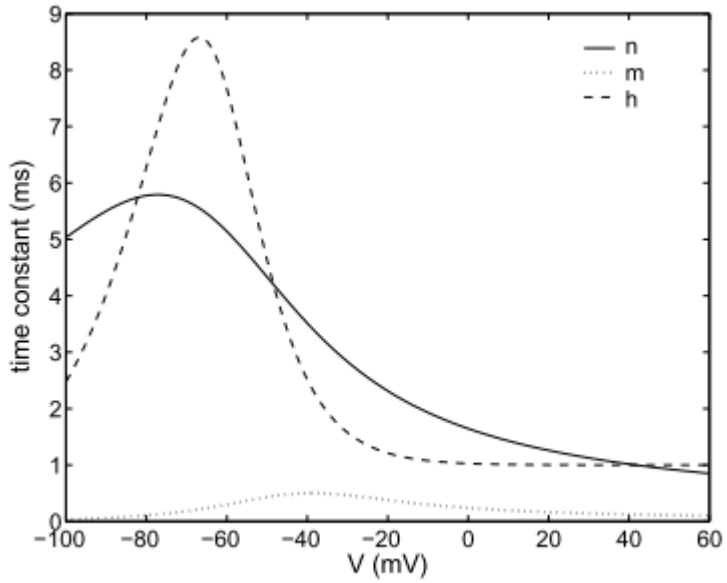

Fig. 3.1. Dependence of time constants upon voltage. *N* is potassium activation gate, *m* is sodium activation gate and *h* is for sodium inactivation gate (adapted from Zeng, 2005).

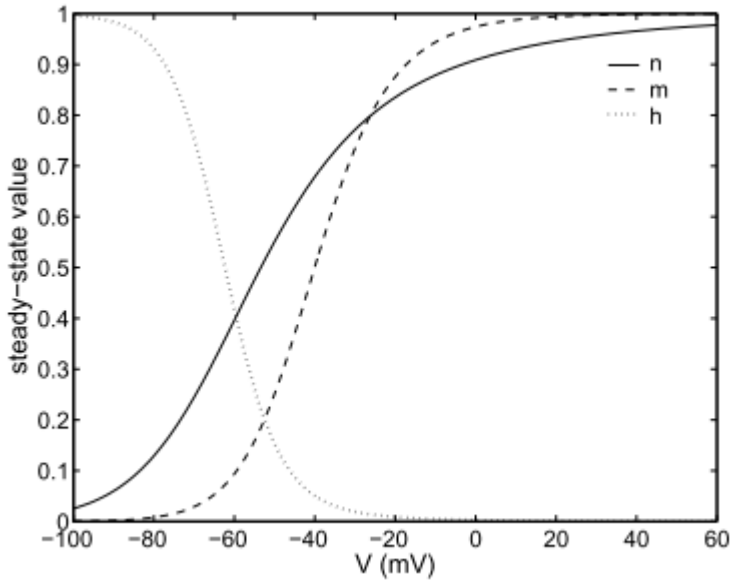

Fig. 3.2. Steady-state values of the gating variables. *N* is for potassium and *m* for sodium activation gate, *h* is sodium inactivation gate (adapted from Zeng, 2005).

The time constants of these gating variables are bell-shaped and τ_m is ten times smaller than τ_h (see *Fig. 3.1.*). In other words, if the membrane potential is suddenly increased, *m* will reach its value in less than a millisecond, while *h* is changed much more slowly. *Fig. 3.2.* is showing the steady-state values of *m, n* and *h*. As could be expected, the activation variables *n* and *m* increase the conductance monotically with membrane depolarization, while *h* is decreasing and around -20mV the inactivation stops completely. In conclusion, the increase in sodium conduction upon depolarization is quite rapid compared to the inactivation process and the resulting ion flow is given by combination of both.

2.3.3 Final model

All remaining ion currents besides sodium and potassium were labeled as „leakage“ by Hodgkin and Huxley. Their conductance, g_{leak}, has a constant value of 0.3 mS/cm^2 and is independent of the membrane potential. The complete model is then described by the following nonlinear differential equation:

$$C_m \frac{dV_m}{dt} = \bar{g}_{Na} m^3 h (V - V_{Na}) + \bar{g}_K n^4 (V - V_K) + g_{leak}(V_{rest} - V) + I_{inj}(t) \qquad (19)$$

Total current across a patch of a membrane. I_{inj} is the current injected by an electrode at a given time, V is the actual membrane potential, V_{rest} is resting potential, g_{Na}, g_K and g_{leak} are conductances multiplied by gating variables for sodium (m, h) and potassium (h) channels (A. L. Hodgkin & Huxley 1952).

The model proposed by Hodgkin and Huxley can now be considered one of the greatest breakthroughs in biophysics of the 20th century. Eversince it has been used for a vast number of simulations of neuronal dynamics and the accompanying phenomena (Hassard 1978; Miller & Rinzel 1981; Lee et al. 1998). Generally, the model allows us to investigate the action potentials as such, the refractory period with the recovery of sodium and potassium channel conductances, and the ability of the neuron to integrate the incoming pulses and to generate an output (Abbott & Kepler 1990). On the contrary, it does not take into account the more complex geometries of some axons and dendrites, neither does it pay attention to other channel types than the sodium and potassium. Furthermore, these equations are purely deterministic, which does not completely correspond with real cells - the neuronal behaviour cannot be precisely predicted because of various types of the intrinsic noise (see the following chapter). Therefore, adjustments to the model have been made to extend the possible applications for theoretical research (Strassberg & DeFelice 1993; Pospischil et al. 2008).

2.4 Intrinsic neural noise

2.4.1 Noise and its role in CNS

Intrinsically, the neuronal activity has a stochastic character, which is generally called *neural noise*. There are more sources of such noise, yet this work is aimed at the membrane characteristics and therefore will only concentrate on the random fluctuations of the membrane potential.

Before the patch-clamp technique became widespread, analysis of membrane current noise was an efficient tool for the research of ion channel properties. In the recent years, this method has been mostly replaced with single-channel recordings, but the noise interpretation can be still used for individual postsynaptic or low conductance

ion channels or for estimation of the way the noise influences information processing in the nervous system (Traynelis & Jaramillo 1998). The main assumption was that noise reduces the amount of information processed by neurons (Manwani & Koch 1999a; Manwani & Koch 1999b). Nevertheless, it has been shown that certain forms of noise, for example the stochastic resonance, can increase the sensitivity of the system towards weaker inputs (Collins et al. 1995). Some studies have also shown the role of these intrinsic fluctuations in human perception and cognitive impairment during aging or neurodegenerative diseases (Welford 1965; Kail 1997).

An interesting example can be the recent theories discussing that either elevated (Simmons et al. 2009) or decreased (Davis & Plaisted-Grant 2014) levels of endogenous noise can lead to cognitive dysfunctions in autism. On one hand, high amount of neural noise might increase the signal/noise ratio and thus lead to impaired sensitivity towards nuances in the visual perception, such as faces recognition (Simmons et al. 2009). On the other hand, too little noise could eliminate the ability to ignore subtle changes between objects and contexts and thus to categorise the surrounding environment (Davis & Plaisted-Grant 2014). In summary, the exact influence of noise on the intercellular as well as the whole-brain level is yet to be clarified and one way to achieve this is the computational analysis technique used in this work.

2.4.2 Sources of fluctuations

2.4.2.1 Thermal noise

The electrical charges of all conductors carry with themselves a certain thermal agitation – the so called *thermal noise* (also known as *Johnson noise*, or the *white noise).* It sets the lowest amount of noise present in every system and can only be reduced by the decrease of temperature or the system bandwidth (Johnson 1928; Manwani & Koch 1999a). However, this noise source has been found to have only a negligible effect on the neuronal dynamics and thus will not be further addressed (van Rossum et al. 2003).

2.4.2.2 Synaptic background noise

Another source of random fluctuations comes from the synaptic activity - more precisely we are talking about the effect of converging outputs from a large number of presynaptic neurons. This leads to voltage fluctuations resembling a random

behaviour and is therefore called *synaptic background noise.* Although it is not a true noise by definition, but rather a result of a large number of different incoming signals, together with the truly stochastic synaptic transmission it indeed approximates a random character. This type of noise is the most influential noise type in dendrites and neuronal soma (Calvin & Stevens 1968). It has been proven to affect the spike timing precision (Paré et al. 1998; van Rossum et al. 2003), but, at least in CA1 hippocampal neurons, also to enhance the detection of a low-level signal - a phenomenon known as the *stochastic resonance* (Stacey & Durand 2001).

Synapses can also cause voltage oscillations either due to a random vesicle releases without any previous stimulation, or due to the variability within the release of vesicles containing neurotransmitters. Some parts of CNS, such as the CA3 region of hippocampus, have only one release zone with a probability of vesicle release between 0.1 – 0.9, and also the different sizes of the quanta can be responsible for the variability in the *excitatory postsynaptic currents* (EPSCs) (Bekkers et al. 1990; Bekkers & Stevens 1995; Murthy et al. 1997). These two factors have been shown to have the major influence on the oscillations in spike time precision in the CA3 area (Kuriscak et al. 2012).

Considering the signal perception by neurons, the synaptic background noise has an undoubtable impact on the final information processing. The combination of inputs from a large amount of presynaptic neurons creates a constant "hum", which increases the signal to noise ratio. Whether this is by all means an undesirable process is still being discussed. Nevertheless, our object of study is the spike propagation along excitable membranes such as the axons, and here the synaptic noise is not as prominent as the noise caused by the stochastic channel gating.

2.4.2.3 Ion channel noise

Hodgkin and Huxley (A. L. Hodgkin & Huxley 1952) summed the behaviour of all ion channels of a certain type into one number expressing the fraction of the open units. However, this is a simplification which does not reflect the micro-oscillations in conductances caused by the stochastic switching of individual channel gates between closed and open states. (This means that even when the membrane is in the resting potential, despite the voltage-gated Na^+ channels are considered closed, some

of the channels open for a fraction of time and thus enable flow of current). This is called the *stochastic ion channel noise* and it is the third major source of the fluxes in the membrane potential (Hille 1978).

An example of how the rising and falling channel conductances differ from the mean behaviour is illustrated in *Fig. 4. a)*. Here we can see a simulation of five different voltage-clamp responses of 1800 potassium channels (conductance per single channel is 20 pS; T = 6 °C; V_m = -40 mV; average conductance is 7.6 nS). In comparison, the synaptic background noise demonstrated in *Fig. 4. b)* is considered more complex as it is formed of multiple independent sources. This figure shows five examples of noise from 1000 independent synaptic inputs with the mean coductance of 9.1 nS (White et al. 2000).

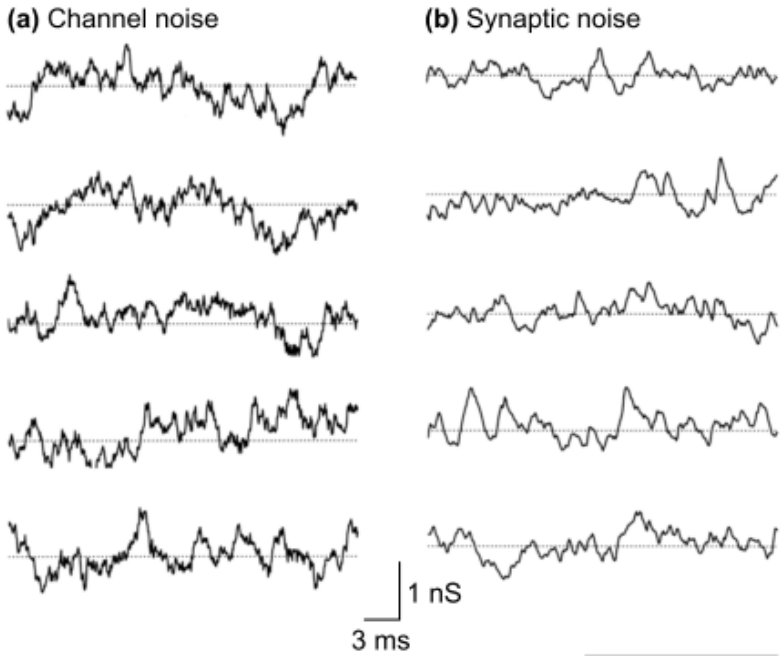

Fig. 4. Simulation of channel noise. Five independent samples of fluctuating conductances of voltage channels **(a)** or the synaptic background noise **(b).** The horizontal lines indicate the average steady-state conductances (adapted from White et al. 2000).

Although the neuronal reliability is considered to be mostly limited by the synaptic noise, there are cases where the effect of ion channel noise prevails. Firstly, it is the situation when there are too many independent excitatory inputs and lack of inhibitory inputs in the synapse, which might lead to a decreased variance of the membrane current (van Vreeswijk & Sompolinsky 1996). Secondly, with a relatively small number of persistent ion channels (10^4 and less), the coefficient of variation

in membrane current increases, as was demonstrated in a simulation of Na^+ channels in neurons of entorhinal cortex (see *Fig. 5.*). The same study showed that the properties of sodium channel conductance cause a shift of voltage from values near the resting potential towards spike threshold upon its activation (White et al. 1998).

Fig. 5. Simulated responses of neurons in the entorhinal cortex varying with different number *N* of persistent Na+ channels. g_{Na} = 0.25 mS/cm2, *Exp.* is a response recorded experimentally and matches with *N* = 4 800 (adapted from White et al. 1998).

The importance of ion channel noise can be demonstrated with an example of its practical implications in the improvement of cochlear implants, devices used to reduce the severity of hearing loss (Rubinstein & Miller 1999). Under physiological conditions, both the release of neurotransmitters by inner hair cells, as well as the spontaneous activity of auditory nerves have a stochastic dynamics, creating a noisy environment which can be beneficial in terms of information coding (Johnson Andnelson & Kiang 1976; Sewell 1984; Collins et al. 1995; Parnas 1996). The electrical stimulation of patients with hearing loss diminishes the spontaneous activity and might cause tinnitus or other complications (Kiang & Moxon 1972). The current research aims at addition of a high-frequency stimulation into the implants, which could amplify the intrinsic neuronal noise and optimize the function of auditory nerves, so that it is closer to the natural state (Miller & Matsuoka 1999; Paffi et al. 2015).

In conclusion, the electrical noise from voltage-gated channels as well as from neuronal synapses is provably present and should be taken into account in any credible model of neural dynamics. It is not only a factor limiting the coding accuracy in neurons,

as has been assumed (Zador 1998; Manwani & Koch 1999a). It can also enhance the signal detection under specific conditions (Collins et al. 1995) or broaden the spectrum of neural responses (White et al. 1998). All these properties have been demonstrated either experimentally or using computational models. The following chapter will describe the most common versions of Hodgkin-Huxley equation adjustments used for channel noise analysis.

2.4.3 Modelling channel noise

A relatively simple way to depict the actual kinetics of channel state transitions is to extend the already existent and functional Hodgkin-Huxley equations, as reviewed by (DeFelice 1981). Here the channel kinetics behave according to the Markov Chains Monte Carlo *(MCMC)* model. This model assumes the channel gates to be independent of the others and to be memoryless, i.e. the current switching between states is in no way related to the past transitions. For example, the potassium channels can be in 4 different states, depending on whether 1, 2, 3 or 4 of the *n* gates are open. For each gate there is a probability α that it will open in the next time step, and probability β that it will close:

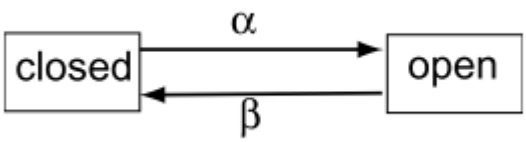

Considering all gates are behaving independently, the probabilities of the whole potassium channel switching from one state to another are illustrated in *Fig. 6. b)*.

Sodium channels are more complicated. They can occur in 8 different states as they have 3 subunits *m* and 1 inactivating subunit *h.* The channel is open if all *m* subunits are open and the *h* subunit is not blocking the pore. Then the channel transition probabilities are a combination of probabilities for the *m* (α_m, β_m) and *h* (α_h, β_h) subunits (see *Fig. 6. a*)).

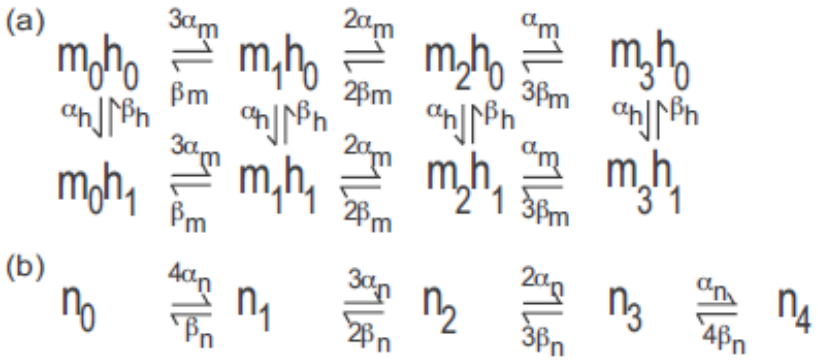

Fig. 6. Markov chains with the gating state transitions for **a)** Na^+ channels **b)** K^+ channels. The m_3h_1 and n_4 are the open (thus conducting) states, $\alpha_{m,h,n}$ is the probability of opening of a gate and $\beta_{m,h,n}$ is the probability of a gate being closed (adapted from Sengupta et al. 2010).

The described probabilities are in fact the voltage-dependent α and β transition rates described in the chapter about Hodgkin-Huxley equations. In a defined number of ion channels, they stand for the fraction of channels which transit between the two given states in a single (0.01-ms) step (White et al. 2000; Sengupta et al. 2010). For example, if there are 100 000 sodium channels and $\alpha_m = 0.02$, then approximately 6 000 (3 x 0.02 x 100 000) channels will switch from state m_0h_0 to m_1h_0 in the next time step. The exact number of channels which would undergo this change would be a random number from a binomial distribution, more specifically the Bernoulli distribution, where the number of trials is n=1 (McCullagh 1984). However, in a large number of channels (as in our case), this binomial distribution is approximated by the Gaussian (normal) distribution. We thus used the Gaussian curves with the mean in the calculated probabilities (multiplied by the overall number of channels N), from which we chose a random number of transitted channels in each time step. The dynamics of this model is the same as the Hodgkin-Huxley's (see equation *19*), except for m^3h and n^4 are replaced with the fraction of open channels. The fluctuation of this number with every time step is then the basic principle of the membrane current noise (Goldwyn & Shea-Brown 2011). If the number of channels $N \to \infty$, then the system behaviour is almost the same as the deterministic type (the noise amplitude is very small), whereas with lower amount of channels, such as 10^4, the noise is much more prominent (White et al. 1998; Austin 2008).

This theoretical model has been used as an alternative to the analysis of experimental single channel recordings via patch-clamp. The patch-clamp technique enables us to observe the current flowing through a single ion channel protein in real time in cells *in vivo*. However, analysing the data collected in this way can be complicated. Firstly, it is possible to only observe one or few membrane patches at once, which does not provide a very complex idea of how the signal is propagating. Secondly, the changes in current or voltage only respond to the conducting or non-conducting states, but do not distinguish between the different non-conductiong conformations. In the recent years, an adjustment of inversed Markov models has been used to estimate the kinetics behind the measurements, yet the practical use is still challenging (Qin et al. 1996; Qin et al. 2000; Tveito et al. 2016).

On the contrary, the theoretical Markov model is flexible when it comes to neuronal type or the amount of compartments observed. We can also change the levels of noise by adjusting the number of channels and compare its influence on action potentials, spike time precision and other phenomena. To obtain relevant results, two main premises must be fulfilled: the neuronal parameters entered into the model must reflect the actual characteristics of real neurons and the mathematical base of the model must be as precise as possible. The former can be simply achieved by comparing the single-channel recordings of the desired neuronal type from different sources and approximate the values. The latter premise has been a subject of discussion over the past decades.

Since 1970s, several models adding noise to the Hodgkin-Huxley equations have been proposed. One of them was suggested by Fox and Lu (Fox & Lu 1994), who derived a set of *stochastic differential equations* (SDEs) to implement the stochasticity into the original model. However, some studies have expressed their pessimism towards this approach due to the emerging discrepancies. One argument was the finding that the rate constants might be actually time-dependent, which would contradict the idea of memoryless channel transitions and eventually influence the channel kinetics (Jones 2006). Another criticism is that the Fox and Lu's algorithm does not precisely describe the behaviour of channel subunits due to certain generalisations (Bruce 2009). Eventually, two recent papers from Goldwyn et al. evaluated the Fox & Lu's works

together with other current models and, based on experimental comparisons, concluded that the channel SDE model is (with certain adjustments) the best option. We therefore chose this adjusted version as the basis of the experimental part of this thesis (Goldwyn & Shea-Brown 2011; Goldwyn et al. 2011).

2.5 The neural code

The biophysical description is useful if we want to understand how neurons modify and integrate different signals. However, the meaning of the code which is actually transferred in the vast number of inputs and outputs remains a mystery. In some neural circuits, we can already successfully observe the flow of information as we now know what role do the neurons approximately have. Among the most approachable circuits in this matter is the sensory system. All the modalities we perceive are converted into action potentials which must quickly and comprehnesively update our idea of the outer world. To better understand what is happening, we must investigate the way individual neurons code different stimuli, in other words the *neural code* (Borst & Theunissen 1999).

The first attempts to find the relation between neural code and stimuli (Helmholtz 1885; Adrian 1928) revealed that the character of a stimulus is connected with neural activity, such as the frequency of AP, and that the neurons adapt upon a constant stimulation. Subsequently, it was found out that single neurons are more selective towards certain types of stimuli than to others (Barlow 1953), and significant progress was also brougth with the beginning of *cortical mapping*, enabling the localisation of neurons which are functionally related (Mountcastle 1956).

The statistical significance of how neural responses vary with different stimuli is measured by *the information theory*, first proposed by Shannon (Shannon 1948). According to him, a key measure of theory of information is the so called *Shannon entropy* - the amount of uncertainty of a certain variable. In neuroscience, the upper limit of information which can be encoded by a neuron is given by the *entropy of spike pattern.* The real amount of information which can be transferred by the neuron between the input and output is always lower than this entropy and depends on its reliability to propagate an AP (Borst & Theunissen 1999).

The possible coding schemes have been under intense discussion. It is clear that neurons use more ways to represent information due to their limited capacity of responses during a very short time period. The following list summarises the generally accepted mechanisms, although the borders are not sharp and some of the schemes can overlap in certain situations.

2.5.1 Rate coding

The rate coding model was first proposed by Adrian (Adrian 1926) and over the years has become a traditional concept of how neurons may represent the majority of (if not all) information. The basic assumption is that the more intense the stimulus, the higher frequency of action potentials follows. The timing of the spikes is not taken into account as it is highly variable due to the always-present channel noise. Therefore, a statisticial approach is often used to describe the coding mechanism with the mean firing rate over a certain time period or per trial. Putting emphasis on the precise number of spikes instead on their temporal position is reasonable in cases where the signal variability is not acceptable and needs to be reduced. One such case is the motor cortex, where the frequency coding enables the muscles to produce smooth and accurate movements (Adrian 1926; Shadlen & Newsome 1998; Stein et al. 2005).

Although the spike frequency is undoubtedly an important (and in some systems the main) carrier of information, a convincingly high number of studies have proven that this scheme is not applicable under every conditions. For example after the synaptic depression, many central synapses are unable to detect changes in constant firing rates of 30 spikes per second or more (Abbott 1997). Also some intracellular recordings from neurons of the visual cortex showed that the spike train transmission is rather unreliable and some of the spikes often fail to propagate (Stratford et al. 1996). For these and similar cases there are other models available, such as the temporal coding (Gautrais & Thorpe 1998).

2.5.2 Temporal coding

In the temporal code scheme, the precise timing of individual spikes is another source of information. According to a number of studies, the spike time precision varies approximately between 1 – 5 ms (Bair & Koch 1996; Berry & Meister 1998; Liu et al.

2001), but in the auditory and other sensory pathways can be precise on the scale of tens of μs (Joris 1996; Rokem 2005). While the rate coding theory assumes these fluctuations to be a mere result of noise, the temporal coding model considers them to carry information.

One argument is that if rate coding was the main strategy, the neural networks would have evolutionally developed a more regular firing rate with smaller variability, for it would be a much more ergonomic and less robust solution. Another point is that the relative time differences broaden the spectrum of responses, which has indeed shown to be relevant e.g. in the optical pathways, where temporal coding enables to code specific parameters of the stimuli (Optican & Richmond 1987; Golomb et al. 1994). Similarly, in the gustatory system, temporal coding might be the element distinguishing between two different tastes of the same category (for example two types of bitter) (Carleton et al. 2010).

Special attention has been paid to the delay between the onset of stimulus and first responding action potential – the so called *first spike latency.* Some theories suggest that this is one of the most important coding mechanisms used by the sensory system. For example, according to a study of neural coding in the salamander retina, the very first spikes coming from the "ON" and "OFF" ganglion retinal cells provide (with their timing) enough information for the rough reconstruction of the visual field (see *Fig. 7*.) (Gollisch & Meister 2008). Similar impact of the relative spike latency has been registered in the auditory system (Heil et al. 2011), tactile afferent neurons (Johansson & Birznieks 2004) or the rat olfactory system (Cang & Isaacson 2003). However, while the responses of ganglion cells did not seem to be affected by the retinal noise (Gollisch & Meister 2008), it has been proposed that the neural intrinsic noise (especially channel noise) might influence these latencies in certain cases. Whether this phenomenon could impair the coding capacity in some or all systems has been a subject of research (van Rossum et al. 2003; Ozer et al. 2009; Gilles et al. 2010). In any case, it is possible that the effect of noise is suppressed when signals from multiple neurons are combined, as described by a model called *the population coding*.

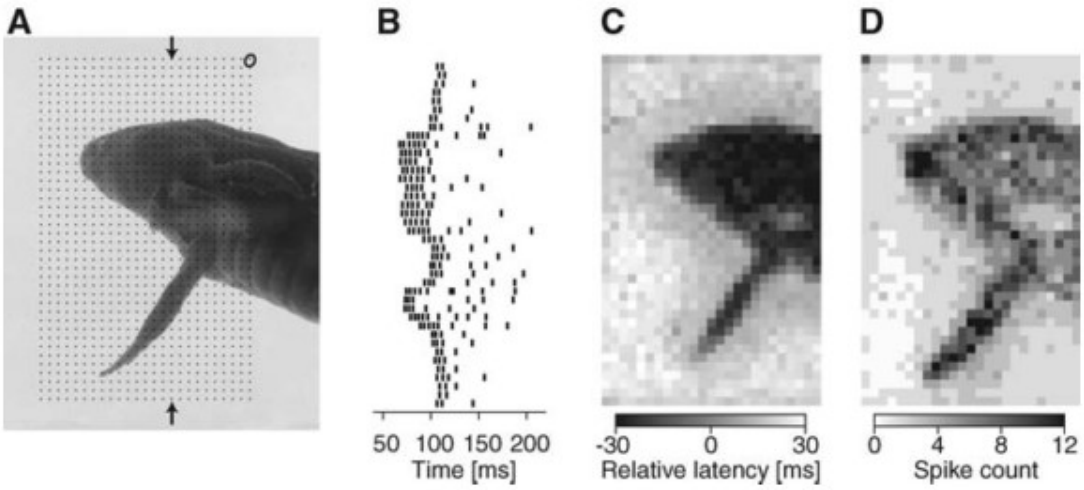

Fig. 7. The response of a salamander's fast OFF ganglion cell after a short display of a natural image. **(A)** Picture of a swimming salamander larva projected on the retina. The ellipse in the upper right corner depicts a sample of the cell's receptive field. The photograph was presented 1000 times and was slightly shifted each time. The grid of dots marks the resulting centers of the receptive field. **(B)** Spike trains of the ganglion cell for receptive-field locations along the column marked by the arrows in (A). **(C)** A gray-scale plot of the differential first spike latencies on single-trial presentations at the locations marked with dots in (A). The reference latency was chosen as the average value at all locations. **(D)** Corresponding gray-scale plot of the spike counts (adapted from Gollisch & Meister 2008).

2.5.3 Population coding

If the activities of multiple neurons together contribute to a full representation of a certain stimulus, we are speaking about *population coding*. If we have N number of independent neurons encoding the same property of a stimuli, the signal reconstruction is improved by $\sqrt{N}$. If these neurons are correlated, the contribution is smaller, yet the network becomes more resistant towards intrinsic noise due to increased redundancy in the system (Bialek et al. 1997). This encoding is especially beneficial in the motor and sensory cortex where they can represent specific direction. Each cell here works as a vector with its own preferred direction and the resulting vector sum of all inputs represents the real direction in which the body or a seen object is moving (Georgopoulos et al. 1986; Lee et al. 1988; Maynard et al. 1999).

A similar coding scheme also including more neurons is *the sparse coding*. Here each stimulus is encoded by a strong activation of a small number of specific neurons. This is also used by the sensory system, as one of the highlights is the increased memory

capacity and thus pattern storage (Willshaw et al. 1969; Olshausen & Field 2004). According to some other works, sparse coding might be also helpful in the formation of associations with the use of learning rules such as the Hebbian learning (Baum et al. 1988; Palm & Sommer 1996; Kuriscak et al. 2015). Nevertheless, all these assumptions are based on the premise that neurons work as classifiers, assorting the inputs into discrete output signals. Some recent hypotheses however suggest that the brain might be rather using certain predictive models or different probabilistic coding (Spanne & Jorntell 2015). If some of these theories shows to be true, then the whole concept of sparse coding will have to be reevaluated.

Although we are still far from being able to read the language of the brain, certain models describing the probable principles of neural code have been proposed in the recent years. We now assume that neurons might transmit information through the mean number of spikes, their relative timing or latency and that combination of outputs from multiple cells can also depict some unique attributes. It is also becoming evident that the impact of neuronal noise on the precision of signal propagation is not negligable. The experimental part of this thesis is therefore trying to closely investigate some possible situations in which the channel noise indeed influences the signal transfer along axons and to relate the findings to the up-to-date discoveries in this area.

3 Aims of the study

Over the past decades, an intense study of brain cells and neural networks has been slowly uncovering the way we process information and incorporate it in our minds. However, a large proportion of phenomena observed within the neural dynamics remains unexplained. One such example is the intrinsic neural noise, a constant source of randomness which we believe to be an influential aspect of the system. This has been proven not only on the subcellular level, where it increases variability of signal generation and transmission, but also on a large scale as a potential factor in certain diseases and cognitive (dis)abilities. Therefore, we decided to research this area using a theoretical computational model – an approach nowadays widely respected for its advantages in situations which are experimentally difficult to reach. We concentrated on the ion channel noise, as its behaviour is more predictable than that of the background synaptic noise, and chose the neuronal compartment where this type of noise has a significant impact – the axon. The specific intentions of this study were following:

1. To develop a stochastic compartmental model of a mammalian axon

Despite the number of attempts to simulate the intrinsic channel noise in neurons, there is a lack of detailed models based on the mathematical and statistical methods that have been recently reevaluated as the most precise and plausible. Furthermore, even when such studies occur, very rarely do the authors provide their source code and it is therefore not reviewable, neither can it be used by other scientists to expand the research.

We therefore aimed at creating a computational model as precise as possible due to the latest findings to obtain scientifically relevant data. The second intention was to make the model available for everyone by using a user-friendly software (MATLAB) and making the code comprehensible and easy to adjust. Publishing the code together with this work could thus be helpful for other theoretically-based experiments in this area.

2. To analyse the influence of channel noise on action potential propagation

Another purpose of our research was to investigate the impact the intrinsic ion channel noise has on various signal transfer characteristics, namely those which have been shown to be involved in information coding, such as the spike time precision, propagation times, interspike intervals etc. Other factors were to be altered to test their importance, such as the amount of myelination, internode lengths, axon diameter, number of ion channels and others. Statistical analysis of othe obtained data should then be compared with the up-to-date research and possible large-scale implications would be hypothesised.

4 Materials and methods

The intense progress in modern technologies has enabled us to develop new ways for exploration of the nervous system. Be it the magnetic resonance imaging, EEG or the patch clamp technique, many new methods provide us with digital data and their analysis with information technologies rapidly expands our scientific insight. However, computers can be also used to simulate either real-life or hypothetical situations of phenomena which cannot be observed directly or where such different perspective might be beneficial. Our point of interest is in the processes happening on a subcellular, even submolecular level, where the up-to-date experimental techniques still fail to analyse the sample reliably and in detail. Therefore, we chose *computational neuroscience* to mathematically reconstruct the neural dynamics and provide a sufficient model which can be used for analysis of the information theory and the transfer characteristics within the axon.

4.1 Simple Hodgkin-Huxley model

Our first step was to implement the original nonlinear differential equations designed by Hodgkin and Huxley (Hodgkin et al. 1951) into MATLAB program to obtain a deterministic model of a simple spiking neuron. This was done by first inserting

the equations for the opening and closing rates α and β of sodium, potassium and leakage channels (see equations 1O, 11 and 15-18 in the chapter *2.3*.) as well as the differential equations for the probabilities *n*, *m* and *h* (equations 9, 13 and 14 on pages 12 and 13). Next, we set the Na, K and leakage reversal potentials and conductances according to H-H:

x	**Reversal potential E_x (mV)**	**Conductance g_x (mS/cm²)**
Na	115	120
K	-12	36
Leakage	10.6	0.3

The membrane capacitance was 1 μF/cm² (a standard value in neurons) and the resting potential was set at -60 mV. The changes of voltage and current in time were calculated using iterations with a 0.01 ms time step for the whole simulation time (which we varied between 200 – 500 ms). That means, in each time step the α and β rates were calculated, based on them also the *m*, *n* and *h* variables and these were used for the computation of the overall current *I*:

$$I = I_{inj} + g_K \times n^4(E_K - V) + g_{Na} \times m^3 h\,(E_{Na} - V) + g_{leak}\,(E_{leak} - V) \qquad (20)$$

Where I_{inj} is the injected current, g is conductance, E is the reversal potential, V is the actual membrane voltage and n, m and h are the open probabilities for potassium (n) and sodium (m, h) channels.

The voltage change for the next iteration was then calculated using the following equation:

$$V_{(i+1)} = V_{(i)} + \frac{\Delta t}{C_m}\left(\frac{V_{(i)}}{R_a} + I_{(i)}\right) \qquad (21)$$

V is the overall voltage at the membrane, *i* is the current iteration , Δt is the time step, *Cm* is the membrane capacitance, *Ra* axial resistance and *I* is the overall current at iteration *i*. The set of differential equations was solved using the Euler method (Wilkinson 2011).

Such model allowed us to simulate neuronal responses to injections of current with variable amplitudes or duration for a desired time length (see *Fig. 8.*). However, this only served as a deterministic core which was yet to be extended by the stochastic factor, that is the ion channel noise.

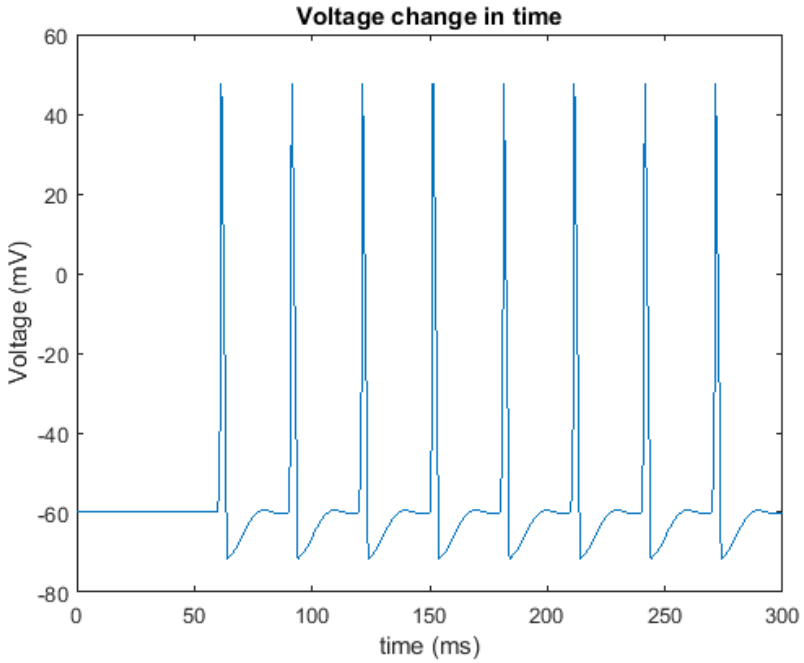

Fig. 8. A sample of a simple spiking Hodgkin-Huxley neuron. The cell was shortly stimulated with injected current (20 nA) after 60 ms of simulation and then again every 30 ms to present its firing activity.

4.2 Adding ion channel noise

The principle of adding ion channel noise into the model is in replacing the m^3h and n^4 variables with the actual fraction of currently open channels. This was done using the method of Markov chains described in the chapter *2.4.3*. The initial assumption was that at any moment, all of the channels are dispersed between 8 (for sodium) or 4 (for potassium) possible states. For every open gate, there is a probability β that it will close in the next step, and for every closed gate, there is a probability α that it will open. Therefore, according to the laws of combinatorics, it is possible to count the probability of transition between any two channel conformations. We calculated all possible transitions and created a *transition matrix* for both sodium and potassium channels

(*Fig. 9.1* and *9.2*.). The possibilities of the channel staying in the same state were left out as it was considered simply as the rest of the total number of channels.

New state → / Initial state ↓	$h_0 3m_0$	$h_0 3m_1$	$h_0 2m_1$	$h_0 m_1$	$h_1 3m_0$	$h_1 m_1$	$h_1 2m_1$	$h_1 3m_1$
$h_0 3m_0$		$6\alpha_m^3$	$6\alpha_m^2$	$3\alpha_m$	α_h	$3\alpha_m\alpha_h$	$6\alpha_m^2\alpha_h$	$6\alpha_m^3\alpha_h$
$h_0 3m_1$	$6\beta_m^3$		$3\beta_m$	$6\beta_m^2$	$6\beta_m^3\alpha_h$	$6\beta_m^2\alpha_h$	$3\beta_m\alpha_h$	α_h
$h_0 2m_1$	$2\beta_m^2$	α_m		$2\beta_m$	$6\alpha_m^3\alpha_h$	$2\alpha_m^2\alpha_h$	α_h	$\alpha_m\alpha_h$
$h_0 m_1$	β_m	$2\alpha_m^2$	$2\alpha_m$		$\beta_m\alpha_h$	α_h	$2\alpha_m\alpha_h$	$2\alpha_m^2\alpha_h$
$h_1 3m_0$	β_h	$6\alpha_m^3\beta_h$	$6\alpha_m^2\beta_h$	$3\alpha_m\beta_h$		$3\alpha_m$	$6\alpha_m^2$	$6\alpha_m^3$
$h_1 m_1$	$\beta_m\beta_h$	$2\alpha_m^2\beta_h$	$2\alpha_m\beta_h$	β_h	β_m		$2\alpha_m$	$2\alpha_m^2$
$h_1 2m_1$	$2\beta_m^2\beta_h$	$\alpha_m\beta_h$	β_h	$2\beta_m\beta_h$	$2\beta_m^2$	$2\beta_m$		α_m
$h_1 3m_1$	$6\beta_m^3\beta_h$	β_h	$3\beta_m\beta_h$	$6\beta_m^2\beta_h$	$6\beta_m^3$	$6\beta_m^2$	$3\beta_m$	

Fig. 9.1. Transition matrix for Na+ channels. The table contains probabilities of the channel switching between the two given states during one time step. α_m and α_h is the probability that gate *m* or *h* will open in the next step, β_m and β_h are the probabilities that gate *m* or *h* will close in the next step. The 0 index means the gate is closed, 1 means it is open. In the $h_1 3m_1$ conformation, all gates are open and *h* is not blocking the pore, that means the channel is conducting.

New state → / Initial state ↓	$4n_1$	$3n_1n_0$	$2n_1 2n_0$	$3n_0n_1$	$4n_0$
$4n_1$		$4\beta_n$	$6\beta_n^2$	$4\beta_n^3$	β_n^4
$3n_1n_0$	α_n		$3\beta_n$	$3\beta_n^2$	β_n^3
$2n_1 2n_0$	α_n^2	$2\alpha^n$		$2\beta_n$	β_n^2
$3n_0n_1$	α_n^3	$3\alpha_n^2$	$3\alpha_n$		β_n
$4n_0$	α_n^4	$4\alpha_n^3$	$6\alpha_n^2$	$4\alpha_n$	

Fig. 9.2. Transition matrix for K+ channels. A table of probabilities of the channel switching between the two states in one time step. α_n is the probability that gate *n* will open in the next step, β_n is the probability it will close. The 0 index means the gate is closed, 1 means it is open. The $4n_1$ conformation is completely open and thus conducting.

The computed probabilities represent a fraction of the total number of channels in the given conformation that will switch to the relevant state. To make this number stochastically fluctuate, in each time step and for every channel state a random

generator picked a number from a Gaussian distribution with the fraction of channels as its mean (see *Fig. 10.*). This number of channels was then substracted from the number of channels in the initial state and was added to the appropriate group.

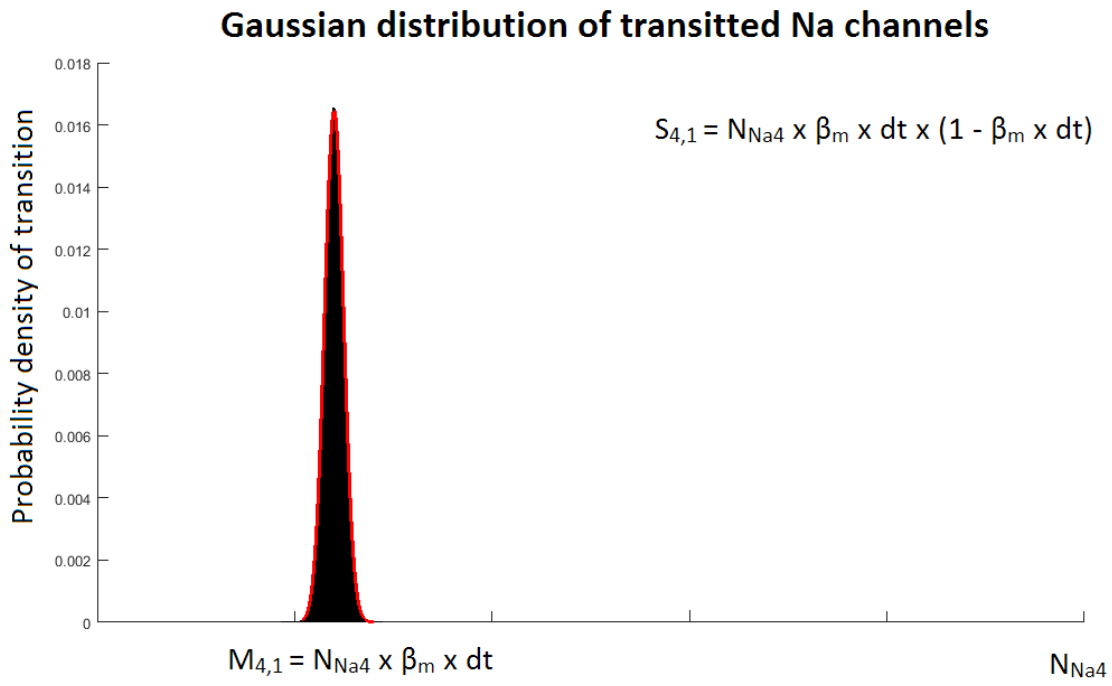

Fig. 10. An example of a normal distribution calculated from the transition probability between state 4 (h_0m_1) into state 1 (h_03m_1) of Na channels. N_{Na4} is the current number of channels in this state, β_m is the probability of transition, dt is the time step (0.01 ms), M is mean and S is variance. This distribution was computed for every transition for both Na and K channels in every time step. A random number generator then picked a number from this distribution, which was the amount of channels that switched into the new state.

The point of our interest was the number of channels in the open conformation ($4n_1$ and h_13m_1), which we divided by the total amount of sodium or potassium channels and obtained a realistic, random fraction of open channels for each time step. This fraction was then used in equation (20) on page 30 instead of the *n, m* and *h* variables. Due to this upgrade, small oscillations within the channel conductances appeared and could be observed in the form of noise (see *Fig 11.*).

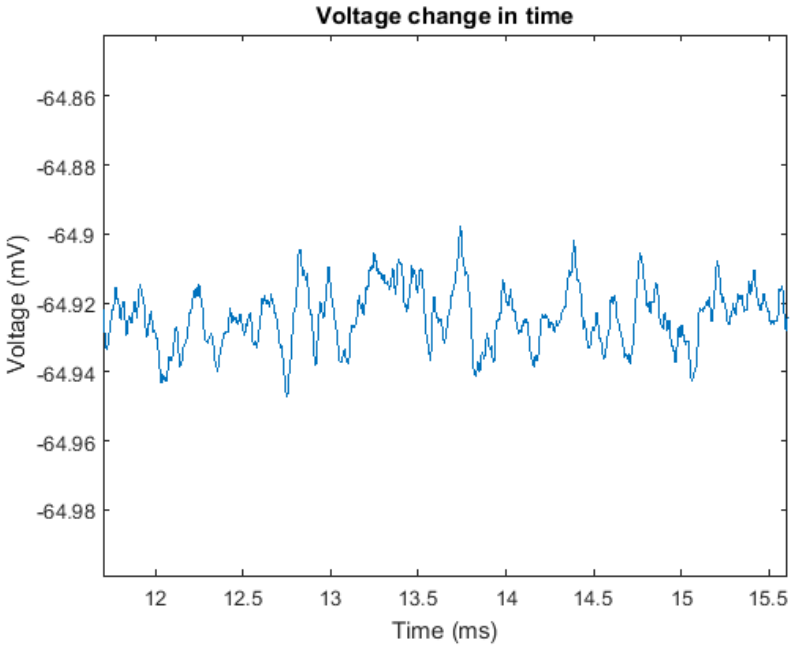

Fig. 11. Model of the neuronal noise from voltage-gated ion channels. Simulated for 10^6 sodium and 10^5 potassium channels.

4.3 Compartmental modelling

During the building of our model, we were trying to reach a simulation in the specific aspects we intended to observe. Since these properties have an electrophysiological basis, using *compartmental modelling* was a reasonable option. In this method, each neuronal part is represented by a single compartment and all units are then electrically interconnected, so that their overall electric behaviour resembles that of a real neuron. This is a simplification based on the cable theory, where each compartment can be seen as a short cable (see page 3). Such component is in our case consisting of the axonal membrane, extracellular and intracellular cytoplasm and ion channels incorporated in the membrane. The actual voltage in the compartment determines the dynamics of ion channels and their activation or inactivation then leads to current alternation flowing across the membrane. A simple scheme of such model is shown in *Fig. 12.* The compartments can be coupled via their intracellular axial resistance *Ra* and each of them can be independently stimulated with current injection. In this way it is possible to form either a linear structure or a branching axonal network.

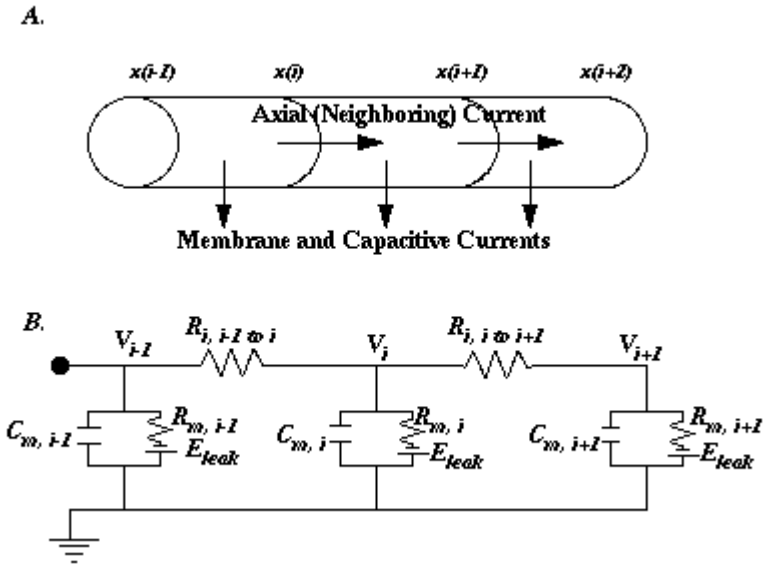

Fig. 12. An example of compartmentalisation of the axon. (A) Three adjacent cables connected through linear resistance term. **(B)** A diagram of a patch of membrane formed of three electric circuits coupled via axial resistance term (here labelled R_i). V_i is the capacitive current, E_{leak} is the passive membrane leakage current, R_m is the membrane resistance, C_m membrane capacitance (adapted from West et al. 1999).

In our study we simulated an unbranched axon with an easily adjustable number of compartments. At each timestep (0.01 ms), the voltage was updated for each segment. This is indeed a sum of the actual voltage at the segment and the overall current (from ion channels and externally injected, the current from the previous and following segment (divided by axial resistance)) . The equation was as follows:

$$V_n(i+1) = V_n(i) + \frac{\Delta t}{C_m}\left\{\left[\left(V_{n-1}(i) + V_{n+1}(i) - 2V_n(i)\right) \times \frac{1}{R_a}\right] + I_n(i)\right\} \qquad (21)$$

Where V is the voltage on the *nth* compartment, i is the current iteration, Δt is the time step, Cm is the membrane capacitance, Ra axial resistance, I is the overall current at the *nth* segment at simulation step *i*. V is in millivolts, I in nanoamperes.

Here each compartment represented a single – plausible segment length of nonmyelinated axon. Furthermore, we increased the accuracy by discerning myelinated internodes and nodes of Ranvier to model myelinated axons. We therefore incorporated between each two nonmyelinated segments one segment with properties resembling those of a real myelinated fibre. The difference from the nodal segments was in their length, capacitance (dependent on the diameter given by the number of myelin sheaths),

membrane leakage resistance (dependent on the conductance of ion channels, which are present in a different densities on the internodes) and axial resistance. This implementation enabled us to adjust further properties, such as the amount of myelination or length of the inernode, and observe the implications on spike propagation.

The current we injected to evoke action potentials was either a rectangular pulse or an α-filter function (*Fig. 13*.). The rectangular pulse enabled us to control the time of generation of an AP more precisely (the depolarization was steeper), whereas the α-filter function was more similar to the postsynaptic *EPSPs* (excitatory postsynaptic potentials) in real neurons (Rall 1967).

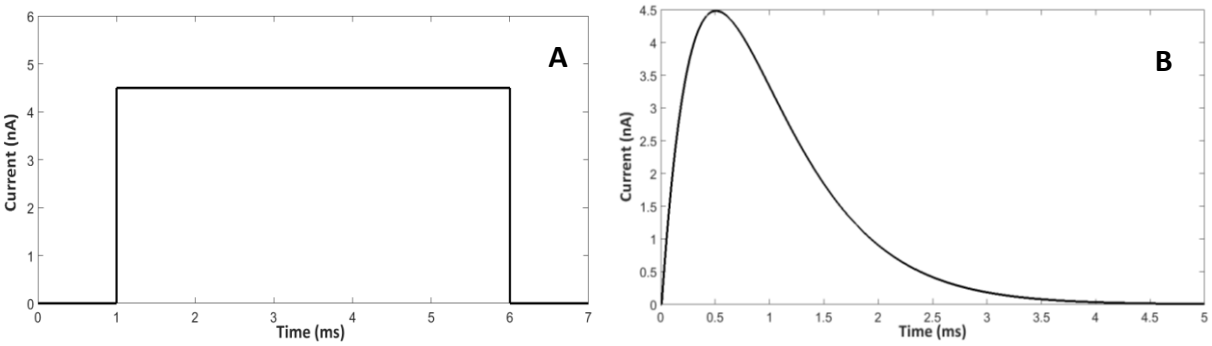

Fig. 13. A demonstration of the two different used forms of injected current. (A) shows a rectangular pulse with duration 5 ms and current amplitude 4.5 nA, **(B)** depicts an α-filter function (duration 5 ms, amplitude 4.5 nA – 2x rheobase) resembling an EPSP of real neurons.

4.4 Model parameters

In the first part of our experiment, we used the parameters of the original Hodgkin-Huxley study on the squid giant axon. Since many od the initial studies of axonal characteristics were performed on the squid axon, there are enough sources of measurements which we compared and approximated the values as precisely as possible (Curtis & Cole 1938; Cole & Hodgkin 1939; Hodgkin et al. 1951). Because this axon type is unmyelinated, all characteristics remained the same along the whole fibre (i.e. there were no internodes). Here is an overview of the key parameters:

$\mathbf{E_{Na}}$	= 115	[mV]	sodium reversal potential
$\mathbf{E_K}$	= -12	[mV]	potassium reversal potential
$\mathbf{E_{leak}}$	= 10.6	[mV]	membrane leakage potential
dt	= 0.01	[ms]	simulation time step
$\mathbf{C_m}$	= 1	[µF/cm2]	membrane capacitance
$\mathbf{g_{Na}}$, $\mathbf{g_K}$	= 120, 36	[mS/cm2]	conductance of Na+ and K+ channels
$\mathbf{g_L}$	= 0.3	[mS/cm2]	conductance of the leakage channels
$\mathbf{R_a}$	= 25	[Ω·cm]	axial resistance
d	= 480	[µm]	axonal diameter
$\mathbf{t_{sim}}$	= 500	[ms]	duration of simulation
$\mathbf{V_{rest}}$	= -60	[mV]	resting membrane potential

A further optimization of our model was the implementation of the kinetics and parameters of a mammalian CA3 neuron. This involved a change in the equations for all α and β rates according to the appropriate kinetics derived by Traub (Traub et al. 1994), as well as an adjustment of certain values and their distinction between myelinated segments and Ranvier nodes. This was a more complicated task as such parameters vary markedly within different studies (Sanders & Whitteridge 1946; Rosenbluth 1976; Graf von Keyserlingk & Schramm 1984; Kuriščák et al. 2002; Ropireddy et al. 2011). We thus estimated the range of plausible options and found an optimum which best suited the model in terms of functionality. The following table involves a summary of some of the used attributes:

$\mathbf{E_{Na}}$	= 115	[mV]	sodium reversal potential
$\mathbf{E_K}$	= -12	[mV]	potassium reversal potential
$\mathbf{E_{leak}}$	= 10.6	[mV]	membrane leakage potential
dt	= 0.001	[ms]	simulation time step
$\mathbf{C_m}$	= 1	[µF/cm^2]	membrane capacitance
$\mathbf{\varrho n_{Na}}$, $\mathbf{\varrho n_K}$	= 2000, 200	[µm-2]	Na^+ and K^+ channel density at Ranvier nodes
$\mathbf{\varrho_{iNa}}$, $\mathbf{\varrho_{iK}}$	= 4, 20	[µm-2]	Na^+ and K^+ channel density at internodes

g_{Na}, g_K	= 15, 17	[pS]	conductance of a single Na+ and K+ channel
g_L	= 0.11	[pS]	conductance of a single leakage channel
l_i	= 0.4 – 3.7	[μm]	length of a Ranvier node
l_n	= 23	[mm]	length of an internode
R_a	= 100	[Ω·cm]	axial resistance
d_a	= 2 - 30	[μm]	axon diameter without myelin
t_{sim}	= 200	[ms]	duration of simulation
V_{rest}	= -65	[mV]	resting membrane potential
T	= 298	[K]	absolut temperature

We also decreased the time step to .001 ms after we had proven that a longer time step decreases precision of the dynamics and yet even shorter intervals are computationally too demanding. Based on the ion channel density and given node length, the overall amount of sodium channels at the Ranvier nodes was approximately 1.1 x 10^6 and about 3.2 x 10^5 of potassium channels. In the internodes, the conductance of a single sodium channel was 0.0008 S/cm^2 and for a potassium channel it was 0.0026 S/cm^2 (Kuriščák et al. 2002; Ritchie & Rogart 1977). We also created an alternative version of this model with a very large number of ion channels (10^{17}), so that the noise was so little it approximated the deterministic model. We then used this version for comparison in some of the experiments.

As for the axon diameters, we varied both the number of myelin sheaths and the inner diameter with values based on experimental studies. The mammalian axon diameters varied between 1 μm and 20 μm (Sanders 1948) and the myelin sheaths were added to obtain a g-ratio (a ratio of inner axon diameter to the outer diameter) close to 0.7 (Chomiak & Hu 2009; Stikov et al. 2015). The thickness of the myelin layers was set according to Graf von Keyserlingk, who proposed that 69 lamelles are approximately 1 μm thick (Graf von Keyserlingk & Schramm 1984). The length of a Ranvier node was at first taken as $l_{internode}/300$ according to Kuriscak (Kuriščák et al. 2002). However, one study of the human optical nerve and cerebral cortex showed that the node length varies between 0.43 – 3.72 μm and, surprisingly, did not find any correlation between this

value and the internode length or axon diameter (Arancibia-Cárcamo et al. 2017). We thus set the node length on 1.5 μm (a mean provided by the paper).

In summary, finding values which would optimally fit our model was complicated due to a large number of studies based on different methods and samples. We thus selected a range of convenient parameters and observed the model dynamics, then decided for the most convenient ones. Because the overall parameter settings mainly corresponded with the real in vivo and in vitro measurements and the dynamics were stable and predictable, we dared to consider the model a credible representation of the mammalian axon.

4.5 Used software

As has been previously noted, we used the program MATLAB (MATrix LABoratory) for our simulation. It is a platform for multi-paradigm mathematical analysis and uses an object-oriented programming language. It was designed by MathWorks in 1980s and eversince has been a popular research tool for both scientists and engineers. We used the version 7.5 released in September 2007 (release name R2007b), no additional toolboxes were needed for our study. The collected data was analysed using either MATLAB or Microsoft Excel 2010.

4.6 Hardware specifications

The program was used on a personal computer with a processor Intel Core i5 with 2 cores, clock speed of 1.60GHz and 4GB RAM. The operating system was Microsoft Windows 10 Pro Version 10.0 (Build 14393) in a 64-bit version.

5 Results

5.1 Stochastic compartmental model of a mammalian axon

Our final model is a simulation of a Hodgkin-Huxley axon with the dynamics and characteristics of a mammalian CA3 neuron. We have successfully implemented the neuronal noise generated by voltage-gated sodium and potassium channels and increased the model precision by adding myelination to the internodes. It is plausible for observation of signal propagation along the efferent fibres as long as tens of centimeters, the overall duration of simulation is adjustable and is thus limited merely by the computer efficiency. All parameters were selected based on either experimental physiological works or values deduced in computational studies. The code is attached in the appendix of this thesis and the MATLAB file will be uploaded together with the electronic version.

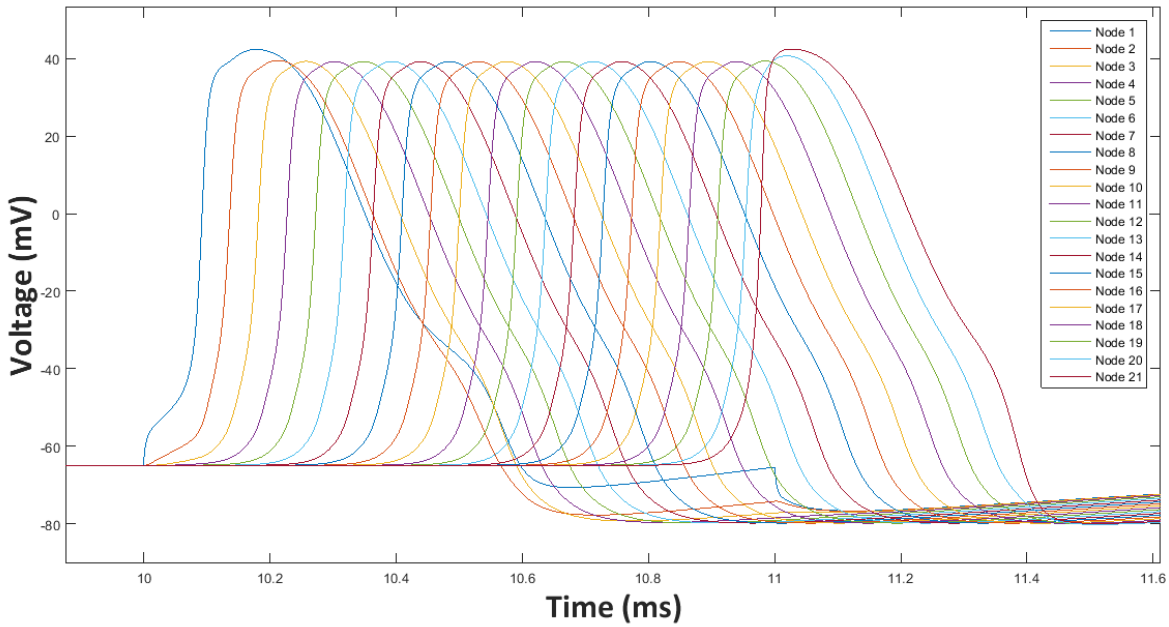

Fig. 14. The spread of an action potential among the nodes of Ranvier. The figure shows a 3-cm long axon consisting of 21 nodes (each painted in a different color), stimulated with a 1-ms long rectangular pulse with 1 nA amplitude. There is an average 46-μs propagation delay (except for the second and last segment, where the delay is 34 μs) between each two neighbouring nodes, with the overall propagation time between the first and last segment being 0.85 ms.

5.2 The influence of ion channel noise on action potential propagation

We first ran a set of experiments on the original H-H model of the squid axon. Here we concentrated on the time of action potential propagation, duration of a single AP and spike time precision depending on the amount of noise. We thus varied the total number of ion channels and mesured the standard deviation (*SD*) of voltage in each trial and each segment. Our results confirmed the fact that the less channels there are, the larger noise (in terms of amplitude expressed as a standard deviation of voltage) they produce (see *Fig. 15*.). Furthermore, we looked at the propagation times of action potentials. The delay between the first and last segment did not change as we shifted the number of channels, but the fluctuations between the AP durations did increase with a larger amount of noise (see *Fig. 16*.). Similarly, the AP duration (with average 0.300 ms, measured from threshold point -50 mV until the return back to the same value) was also more variable in the cases where voltage fluctuations were more prominent (mean SD 5.78 µs in 10^4 channels) than in the less noisy model (mean SD 4.68 µs in 10^7 channels). Also, in the $10^{\wedge 4}$ model, the noise was so large that spontaneous spiking could be observed. All these findings correlate with the idea that increased channel noise impairs the overall precision of the neural code.

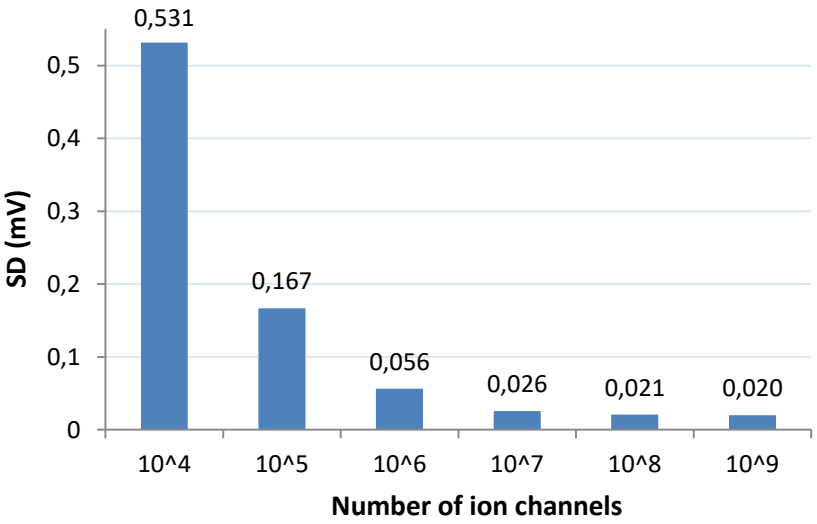

Fig. 15. Standard deviations (SD) of voltage fluctuation dependent on a total number of sodium and potassium channels. The standard deviation was calculated from the voltage of an unstimulated axon with 80 Ranvier nodes during a 200-ms long simulation. Measured at the membrane resting potential -60 mV.

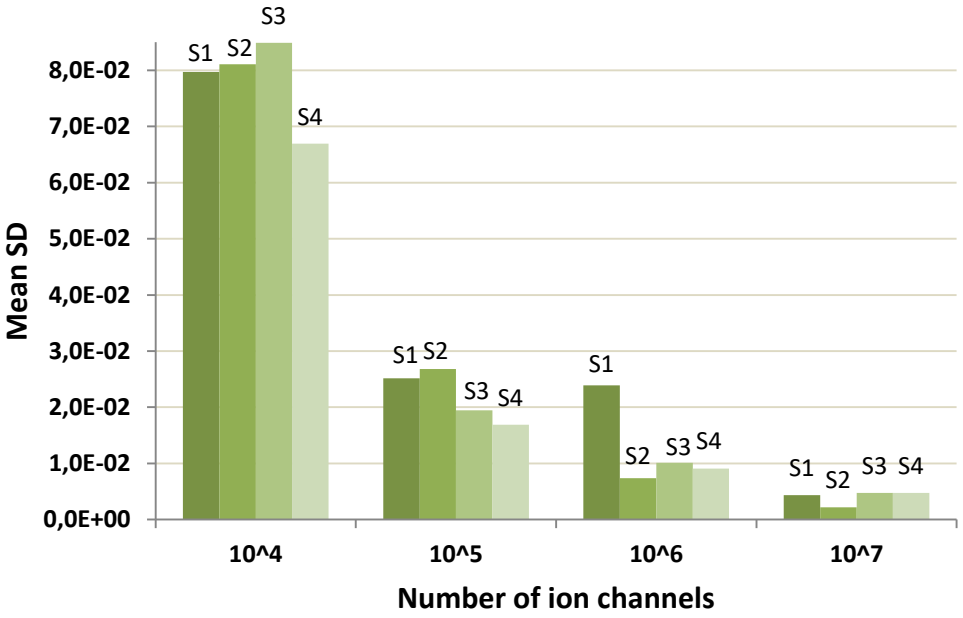

Fig. 16. The dependence of variability of the spike propagation time on the level of noise. The axon was stimulated with 4 rectangular pulses with amplitudes 2.3, 2.4, 2.5 and 2.6 nA and 100-ms separations between the neighbouring pulses. The duration of propagation between the first and last segment was measured - the labels S1-S4 show the mean SD of the propagation times for spikes 1-4 (based on 20 trials). There is a clear correlation between the noise level and the variability of AP propagation time.

The analysis of the CA3 neuron model was more detailed. As mentioned in the Methods section, we compared the AP velocities and SD of propagation times in models with a different time step. The results are summed in *Fig. 17*. The shorter the time step we chose, the slower propagation speed and higher propagation time SD were measured. This, however, does not necessarily mean that the shorter time steps were more precise, as some inaccuracies can emerge due to the rounding error of transitted channels (which is more prominent in shorter time steps). We thus selected the 0.001 ms time step, which was markedly shorter than the fastest processes on the membrane (action potentials, hyperpolarization etc.) and still assured a high computational efficiency of the model.

Time step (ms)	0.005	0.002	0.001	0.0005	0.0001
AP velocity (m/s)	94.3	88.2	82.8	80.9	74.5
SD of propagation time (μs)	0.73	1.22	1.41	2.32	3.94

Fig. 17. The change of AP velocity and SD of propagation time with different time steps. Simulated on an axon 3-cm long with the diameter of 20 μm, stimulated by rectangular 1-ms pulses.

In the resting potential (-65 mV) and physiological values (10^6 Na^+ and 10^5 K^+ channels), the mean amplitude of the noise was 0.051 mV and mean SD was 0.0093. The maximum firing frequency of an axon 20 µm wide (and 3 cm long) was 1 000 Hz with a tonic stimulation (with 6.5 nA amplitude) and 950 Hz with a phasic stimulation with 6-nA rectangular current pulses, each 0.5 ms long. The SD of AP propagation time had an ascending trend with the increasing axon length, indicating a distortion of the spike pattern precision during propagation (*Fig. 18.*).

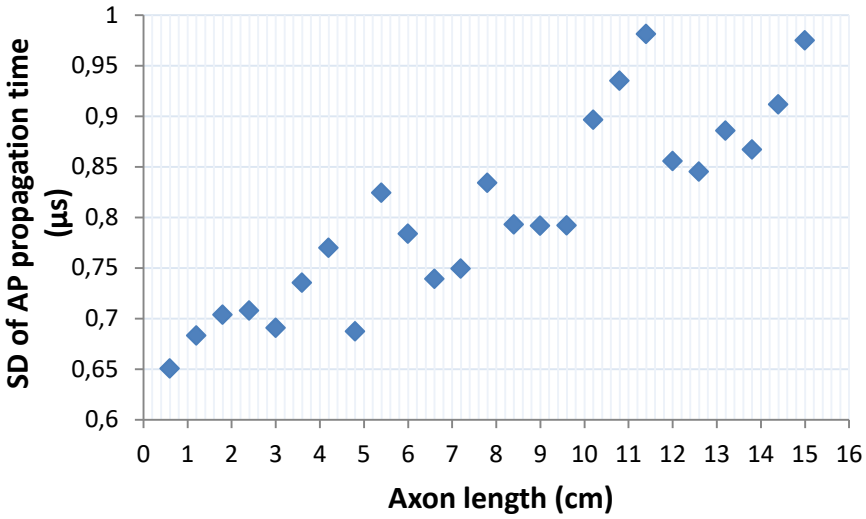

Fig. 18. SD of AP propagation time along the axon. Measured on an axon with a 20-µm diameter, stimulated by 5 1-ms long rectangular pulses temporaly separated by 100 ms. The SD of a 3-cm long axon was 0.69 µs, whereas the SD of the propagation time of a 15-cm long axon was 0.97 µs, indicating a progressive distortion of spike temporal pattern along the axon.

We first varied the axon diameter (together with myelination to keep the g-ratio around 0.7) to observe changes in the spike propagation time (AP velocity) and variability of the temporal precision of APs. The simulated cable was 10 cm long, but the internode length was varying along with the diameter according to the ratio $l_{internode} = 146 \cdot d_{axial}$ (Tasaki 1959)**.** The AP velocity raised dependently on the increasing diameter. A trend analysis of this data showed that the increase is most likely polynomial (R-squared value 0.9995), since it showed the highest confidence compared to the exponential (R-value 0.8831), linear (R-value 0.9977), logarithmic (R-value 0.8375) or power (R-value 0.9989) trendlines. Furthermore, the propagation speed of a 20 µm wide axon was approximately 22 x faster than that of an axon 1 µm thin (*Fig. 19.*).

We also measured the standard deviation of the changing temporal pattern of spikes during propagation. This SD (*Fig. 20.*) thus represents the decrease of spike temporal precision along the decreasing axon diameter. The most rapid increase of SD was evident in the range between 10 – 1 μm (SD 4.7 μs for a 1-μm diameter and 1.9 μs for a 10-μm diameter), wider axons had the SD closely fluctuating around the mean 1.27 μs.

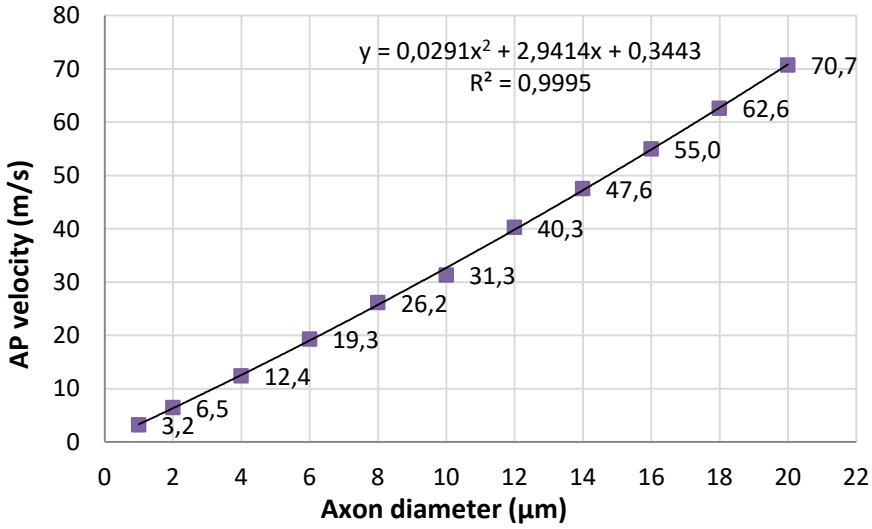

Fig. 19. The relationship between axon diameter and AP velocity. A 10-cm long axon was stimulated with 1-milliecond rectangular pulses with amplitudes between 0.2 - 8 nA (adjusted for each diameter to have an amplitude of 2x rheobase) . The number of myelin sheaths was changed along with the diameter to keep the g-ratio around 0.7. We tested the data for the exponential, linear, logarithmic, polynomial and power trendline and as the most confident one turned out to be the polynomial trendline (equation in the graph, R-squared value 0.9995). Since we have not found any inormation mentioning this trend in the available literature, we consider this finding as new.

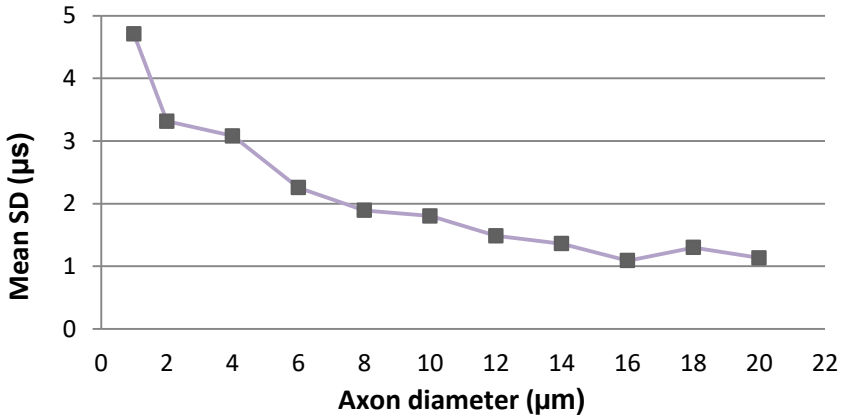

Fig. 20. SD of the temporal spike pattern variability along the axon and its relationship with axon diameter. A 10-cm long axon was stimulated with 1-milliecond rectangular pulses with amplitudes between 0.2-8 nA (2x rheobase). The diameter was changed along with the number of myelin sheaths to keep the ratio of 0.7. Here the mean standard deviation (SD) demonstrates the decreasing temporal precision of AP propagation with decreasing axon diameter. The most rapid changes are between the diameters of 1 – 10 µm, further widening of the axon did not vary the temporal spike pattern as markedly.

Next, we investigated axonal demyelination by comparing the characteristics of fully myelinated axons to those with a gradual loss of myelin sheaths (*Fig. 21*.). (We have linearly increased the membrane capacitance and inversely decrased the membrane leakage resistance along with the increasing diameter). The axon length was 3 cm, diameter 20 µm and the stimulation pulses were remodelled from rectangular into 5-ms α-filter functions (with the amplitude equal to 2x rheobase) to approximate the real postsynaptic signals (Rall 1967). The AP velocity decreased to 68 % of the initial value upon loss of half of the sheaths, whereas the 95-% demyelination lead to a fall of the AP propagation speed down to 11.4 % compared to a fully wrapped axon (*Fig. 21. A*). Another observed parameter was the average duration of individual spikes. Here we found out that with the progressive demyelination, the APs become wider and also the variability of their duration increases. The 95-% demyelination increased the duration twice compared to the initial state, and the SD raised from 9,14 µs to 65,3 µs (*Fig. 21. B*).

Moreover, we ran the same experiment on a nearly deterministic (10^{17}-channels) model to observe any changes in behaviour. However, no major difference was found – the change of velocities differed by 1 m/s and the AP duration and its SD was almost identical with the stochastic version, indicating that the increasing duration might be caused merely by the demyelination without any major contribution from the noise.

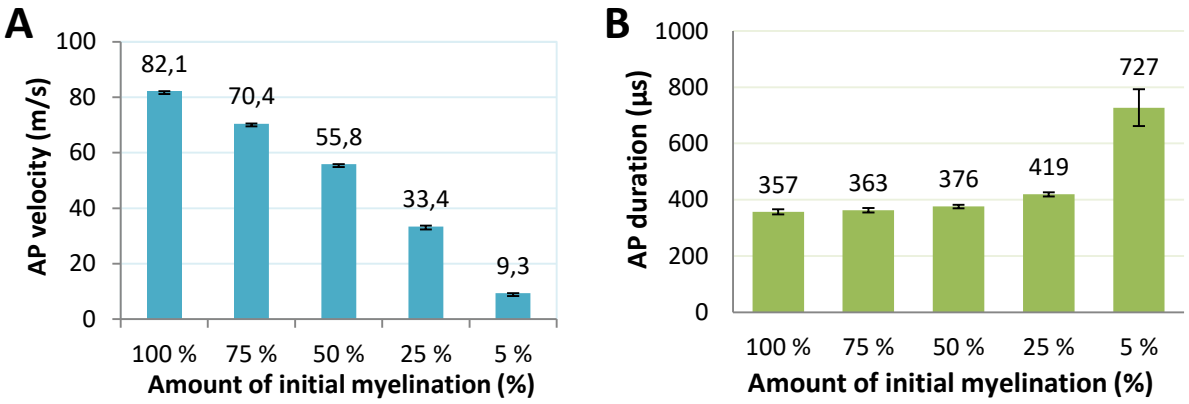

Fig. 21. Relationship between AP propagation and the loss of myelin sheaths. A 100-% myelination corresponded to 230 myelin sheaths for an axon with 20-µm diameter, 5 % equals to 12 myelin sheaths. The length of the measured segment was 3 cm and the stimulation was performed using 5-ms α-filter functions mimicking the excitatory postsynaptic potentials. **(A)** shows the dependence of AP velocity upon demyelinaion, **(B)** demonstrates the change in AP duration with the progressive loss of myelin sheaths.

An interesting observation that we made was that the propagation time of an AP following 2 ms after the previous one decreased by 0.099 ms on average (measured in an axon 3 cm long, 10 µm in diameter). This decrease was less and less prominent with an increasing time separation between the two spikes and was already unchanged if the distance was 10 ms and more. The shift of velocity was variable with axon diameter, in a fibre 10 µm wide the AP propagation speed was decreased approximately by 3 m/s (*Fig. 22. A, B*), whereas in a 20-µm diameter, the velocity was up to 9 m/s slower (*Fig. 23*). This in fact means that a spike can have a "repelling" effect on another spike which follows closely (2 ms and more) after, i.e. the temporal distance between them is growing with their propagation along the axon.

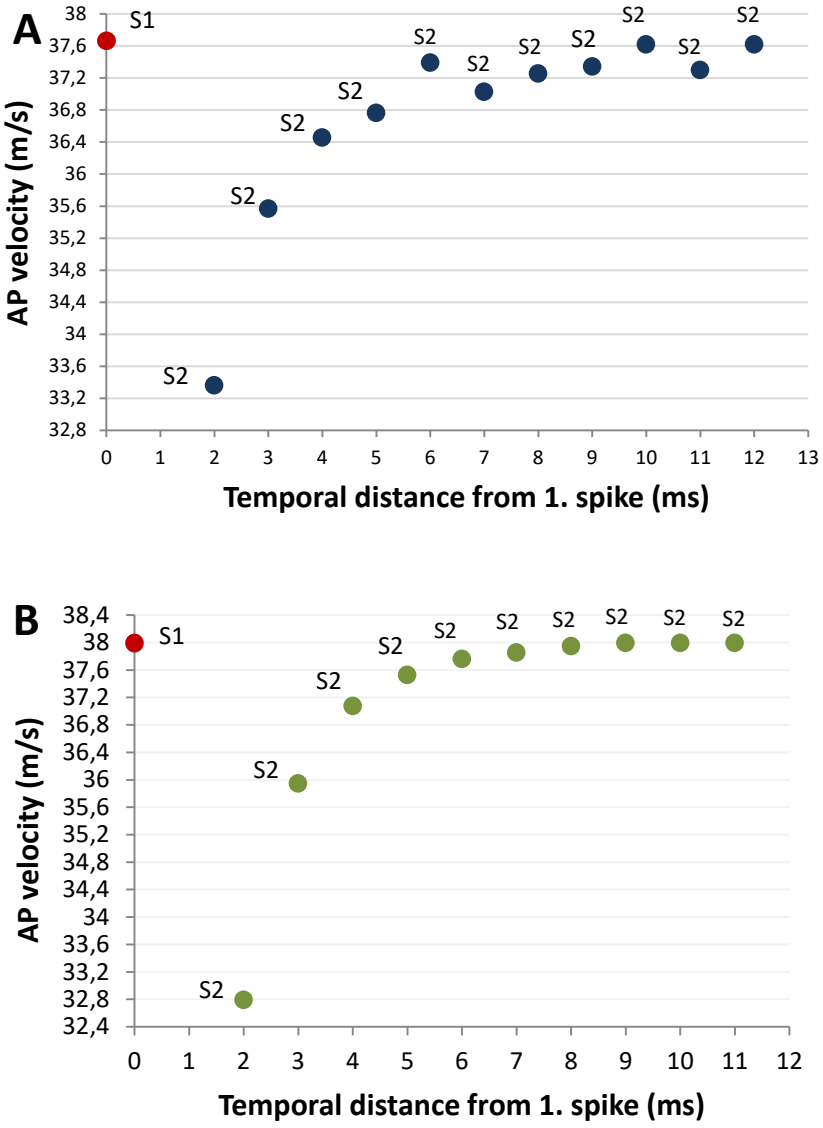

Fig. 22. The change of AP velocity of a spike occuring soon after the previous one. On an axon 3 cm long and 10 μm wide, we injected two rectangular stimuli with the duration of 1 ms and amplitude 10 nA. The first stimulus (S1) was always at the same time, the second one (S2) was fired 2 ms later, then 3,4,5,...,11 ms later. AP velocity shows the propagation speed in proportion to the temporal distance between the two spikes – ISI (*interspike intervals*). **(A)** is an example of the velocity decrease in a stochastic model, **(B)** depicts the same situation in the neraly deterministic model (10^{17} channels).

Such behaviour was visible also in the 10^{17}-channel model, only the change of velocity was more consistent (*Fig. 22. B*). More importantly, in the noisy version the immediate speed drop was smaller by 1.45 m/s on average than that of the 10^{17}-channel deterministic model. This was observed in axons with the diameter between 15 – 20 μm, in narrower fibres this effect was almost negligible. This possibly indicates the role

of the noise in rectifying the repelling effect between spikes – an opposite effect to the widely assumed deteriorating aspects of noise.

Furthermore, the drop of velocity in the following spike could be partially diminisehed by applying a larger stimulus for the second AP compared to the first one. For example, increasing the second pulse 6 x lead to a 30-% decrease of the velocity decrease. This was tested on an axon 3 cm long, with a 20-µm diameter and 1-ms rectangular pulses with intensities between 3 – 30 nA and temporal separation 2 ms (*Fig. 23. A*). We also compared the stimulation by a rectangular pulse to an α-filter function adjusted for each stimulation type to have an amplitude of 2x rheobase, yet the results were very similar.

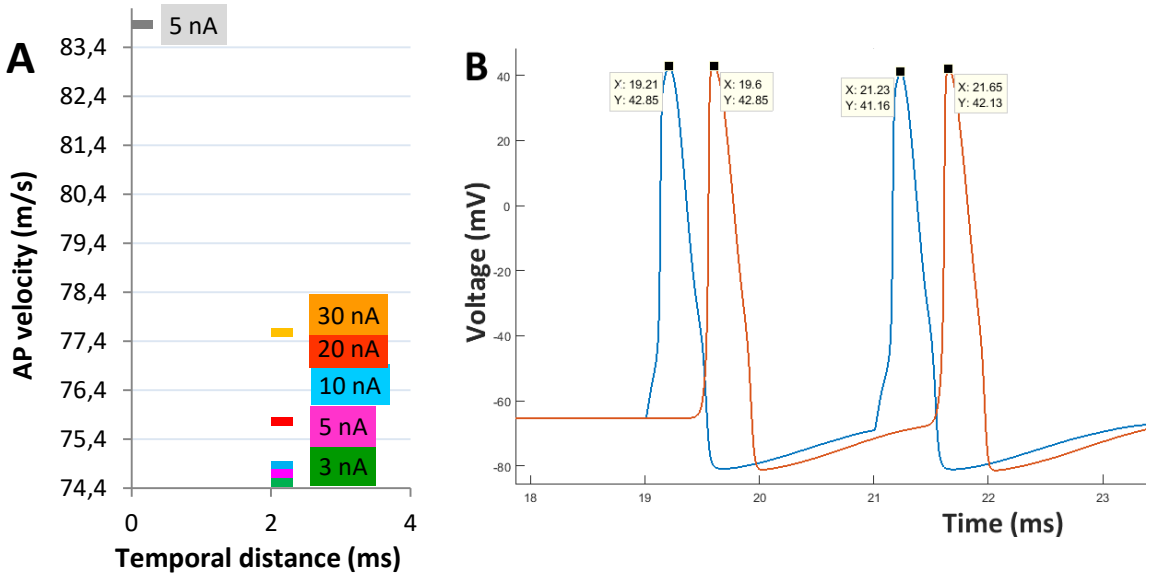

Fig. 23. The AP velocity decrease of the AP fired 2 ms after the first AP. **(A)** A 3-cm axon with 20-µm diameter was stimulated with two 1-ms rectangular pulses varying from 3 to 30 nA. The first pulse remained at 5 nA each time. Applying a much larger pulse compared to the first one lead to a faster spike propagation when compared to a smaller stimulus. **(B)** A demonstration of the velocity drop after stimulation with 5-ms long α-filter functions with the peak amplitude of 2x rheobase. Blue line is the first node, red line is the last node and the markers are showing their peak times (their difference is the propagation delay). In this case, the speed of the first AP was 82.6 m/s and 76.7 m/s of the second one.

At last, we tried to fire a series of 5 APs in a row with 2-ms intervals between them and calculate their velocities. After the first drop, the speeds did not continue falling rapidly, but rather fixated at a certain value (± 76 m/s) and fluctuated around it.

There was thus no return to the initial speed for the observation period. The nearly deterministic model behaved very similarly, but the initial drop was larger by 1.5 m/s compared to the noisy model (*Fig. 24.*).

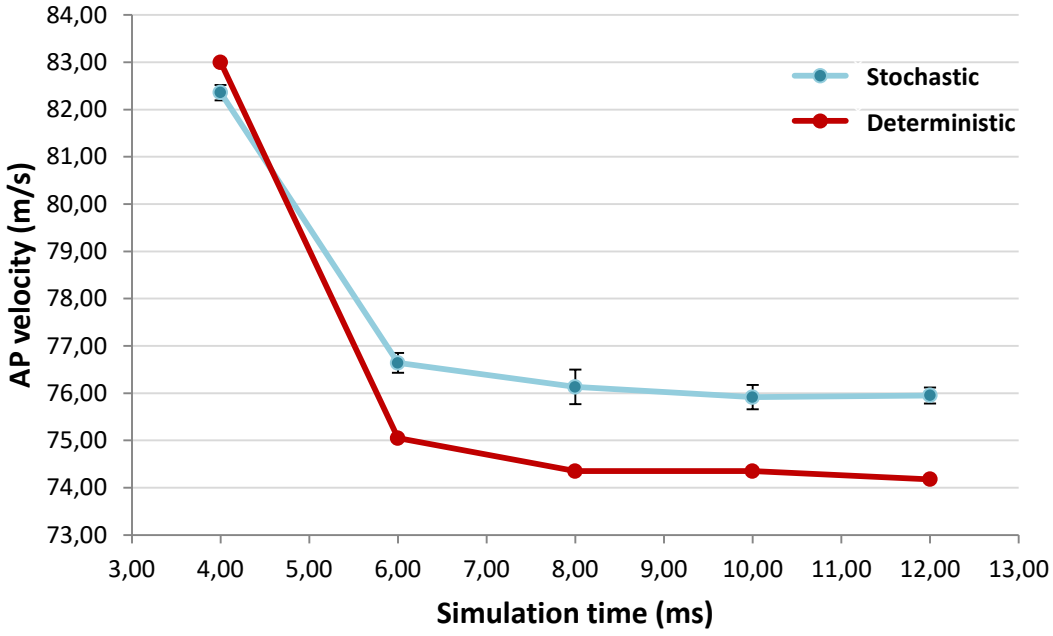

Fig. 24. AP velocities of each of 5 spikes in succession with 2-ms separation. Results of a rectangular pulse stimulation of a 20 µm wide axon and the difference between the stochastic (blue marks) and deterministic (red marks) version. Regardless the amplitudes of pulses, the noisy version always diminished the velocity decrease compared to the deterministic version. This was observed in axons with the diameter varying between 15 – 20 µm. This means in fact, that whereas at the beginning of the axon the APs were separated by 2-ms intervals, their separations at the end changed, leaving e.g the second AP to be repealed from the first AP (approx. by 30 µs after 3 cm of propagation).

6 Discussion

Understanding the way our brain processes information and transforms it into thoughts and memories is one of the greatest challenges in life science. While we have so far gained a lot of knowledge about the cellular, subcellular and even molecular processes, the submolecular scale is still far from being comprehended due to a lack of appropriate technologies enabling its research. One possible approach is the reductionistic model of the neuron, concentrating on its electrical properties underlying information transfer. We have chosen this method to study the transfer characteristics of a mammalian axon, modelled according to its biological background. The main point

of our interest was the stochastic behaviour of voltage-gated ion channels and its influence on axon potential propagation.

We first implemented the traditional Hodgkin-Huxley model into the MATLAB programming language, using a set of nonlinear differential equations solved via the integration Euler method. We then added the ion channel noise via the Markov Chain Monte Carlo method. Due to the use of Gaussian distributions for channel state transitions, the speed of our simulation increased approximately 10^5 x compared to the modelling of each channel transition separately using the MCMC. After a set up of the appropriate axonal parameters, we obtained a plausible model of the giant squid axon.

Here our experiments confirmed the up to date knowledge that the standard deviation of the channel noise effect is dependent on the amount of sodium and potassium channels. The largest amplitudes of spontaneous voltage fluctuations were measured in the version with 10^4 ion channels per a modelled segment, with the axon diameter of 0.5 mm and overall length 3 cm (White et al. 1998). This noise was shown to also influence the precision of action potential propagation, especially the temporal precision and AP propagation time. The standard deviation of the temporal accuracy of propagation in the 10^7 channel noise was only 5 % of the SD measured with 10^4 channels (in an axon 0.5 mm wide and 5 cm long). Similarly, the duration of an action potential was slightly more variable in the noise with higher SD. All these findings correspond with the overall assumption that the channel noise can distort the precision of AP propagation (White et al. 1998; Manwani & Koch 1999a; Manwani & Koch 1999b).

The further extension of our model included the adjustment of channel gating kinetics for a CA3 rodent axon according to Traub (Traub et al. 1994). This was followed by a careful selection of the corresponding parameters based on the available literature. We have also tested various simulation time steps (between 0.005 ms and 0.00001 ms) for the AP velocity and SD of propagation times and selected the value we considered an optimal compromise between simulation accuracy and computational efficacy. The used time step (0.001 ms) allowed a relatively fast simulation and, since the results correspond with experimental findings (as mentioned later), we hypothesise that the transitions of real axonal voltage-gated Na^+ and K^+ channels might as well happen in intervals no shorter than 0.001 ms.

After an initial testing of the model, we concentrated on the three following phenomena.

1. The relationship between axon diameter and AP propagation speed

In this experiment, we varied the axon diameter between 1 – 20 μm along with the internode length and number of myelin sheaths (to sustain a plausible ratio of myelination). The velocity of AP propagation raised rapidly with the increasing diameter and did not turn out to be influenced by channel noise. Based on our results, the AP velocity increased with a polynomial trend (R-squared value 0.9995) according to a quadratic equation $y = 0{,}0291x^2 + 2{,}9414x + 0{,}3443$. Since we have not found any study mentioning this trend, we consider it a new finding, yet emphasize the need of further verification. Lastly, the precision of temporal code propagation had a decreasing course with the decreasing diameter, showing to be most rapid between 1 – 10 μm axon diameter (with SD 4.7 μs in a 1-μm diameter and 1.9 μs for the 10-μm diameter).

2. The change of propagation speed upon axonal demyelination

Another subject of our study was to observe the change of AP velocity with a progressive demyelination, as observed i.e. in patients with multiple sclerosis. Our results show a rapid decrease of the propagation speed along with the loss of myelin sheaths - a 95-% demyelination lead to a drop of the AP velocity speed down to 11.4 % compared to a fully wrapped axon. Furthermore, the mean duration of APs almost doubled after the 95-% demyelination and its variability also rapidly increased. This would mean that in a 100-cm long and 20-μm wide axon (corresponding to wider medullary projections or the A-α sensory fibres), the 95% demyelination would lead to a decrease in velocity from 62 m/s (in a fully myelinated axon) to 7 m/s and the AP duration would more than double from 0.383 ms to 0.791 ms. Such results can predict the possible implications of demyelination caused by progressive neurodegenerative diseases (i.e syphilis, peripheral neuropathy, Wilson's disease) on the AP velocity of affected fibres.

Both the AP velocity and duration during demyelination were also examined in the nearly deterministic (10^{17}-channel) version, yet no significant differences occurred.

Therefore, we conclude that the voltage-gated channel noise does not play an important role in the drop of AP velocity during demyelination.

3. Propagation speeds in APs fired with short temporal separations

Lastly, we evaluated the AP propagation speeds in action potentials fired closely in succession. We found out that the propagation speed of a spike fired after a the first one rapidly decreases by 3 (in 10-μm axon diameter) to 9 m/s (for 20-μm diameter). With the increasing separation between the two spikes, the velocity slowly returns back to the velocity of solitary (well separated) spikes, yet it stays affected until the separation is larger than 10 ms. This could be obviously due to the fact that the membrane is still in a relatively refractory phase (the absolut refractory period was 1 ms for big axons and more, depending on axonal diameter) and thus reacts more slowly to the incoming stimuli.

Furthermore, the drop of velocity could be partially reduced by applying a larger pulse for the second AP than for the first one (approximately by 30 %). We thus conclude that the intensity of stimulus firing the individual AP can influence the way how interspike intervals are altered during propagation, which can possibly influence the spike pattern as recieved by recipient (postsynaptic) neurons.

Interestingly, the comparison between the stochastic and deterministic (10^{17}-channel) model showed that the noisy version can diminish the initial decrease by 1.45 m/s, indicating a rectifying role of the channel noise in certain propagation characteristics. This was however observed only in axons with the diameter between 15 – 20 μm. In summary, we hypothesise that while the short temporal separation of two spikes has a “repelling“ effect on the second spike (i.e. their temporal distance increases with propagation along the axon), the ion channel noise partially reverses the second spike repulsion by approximately 1.45 m/s in a 2-ms separation time. Since we have not found any similar references in the available literature, we assume these results as novel.

7 Conclusion

In summary, we have created a Hodgkin-Huxley model of the mammalian CA3 axon with implemented voltage-gated channel noise in a comprehensible code in MATLAB (see appendix). This model is based on stochastic differential equations solved using the integration Euler method. The channel noise was modelled via Markov Chain Monte Carlo method, speeded up by replacing the Bernoulli binomial distributions of channel state transfers with Gaussian distributions. Such model is efficient and reliable and can serve for further experiments in this area.

From the set of experiments we ran on this model we demonstrated and can conclude the following:

1. The AP velocity increases with larger axon diameters, possibly with a polynomial trend. The biggest variability of spike temporal pattern was measured in diameters between 1 – 10 μm wide.

2. A simulation of progressive demyelination showed a decrease in AP velocity and prolonged AP duration with loss of myelin sheaths. However, we did not observe any effects caused particularly by channel noise.

3. A relatively interesting finding is the fact that APs fired within intervals as short as 2 ms have a slower propagation speed compared to those that occur alone. Furthermore, this decrease of velocity can be partially decreased with a larger amplitude of the second pulse and the channel noise also shows to compensate the speed drop compared to a nearly deterministic model (10^{17} channels). This could be one of the potentially interesting effects of the voltage-gated channel noise on axonal input-output characteristics.

8 References

Abbott, L.F., 1997. Synaptic Depression and Cortical Gain Control. *Science*, 275(5297), pp.221–224.

Abbott, L.F. & Kepler, T.B., 1990. Model neurons: from hodgkin-huxley to hopfield. In *Statistical mechanics of neural networks*. Springer, pp. 5–18.

Adrian, E.D., 1928. The Basis of Sensation. *British Medical Journal*, 1(4857), p.287.

Adrian, E.D., 1926. The impulses produced by sensory nerve-endings: Part I. *The Journal of physiology*, 61(1), pp.49–72.

Arancibia-Cárcamo, I.L. et al., 2017. Node of Ranvier length as a potential regulator of myelinated axon conduction speed K.-A. Nave, ed. *eLife*, 6, p.e23329.

Austin, T.D., 2008. The emergence of the deterministic Hodgkin-huxley equations as a limit from the underlying stochastic ion-channel mechanism. *Annals of Applied Probability*, 18(4), pp.1279–1325.

Bair, W. & Koch, C., 1996. Temporal precision of spike trains in extrastriate cortex of the behaving macaque monkey. *Neural Computation*, 8(6), pp.1185–1202.

Barlow, H.B., 1953. Action Potentials From the Frog's Retina. *Journal of Physiology*, 119, pp.58–68.

Baum, E.B., Moody, J. & Wilczek, F., 1988. Internal representations for associative memory. *Biological Cybernetics*, 59(4), pp.217–228.

Bekkers, J.M., Richersont, G.B. & Stevens, C.F., 1990. Origin of variability in quantal size in cultured hippocampal neurons and hippocampal slices (miniature synaptic currents/patch clamp/brain slice). *Neurobiology*, 87(July), pp.5359–5362.

Bekkers, J.M. & Stevens, C.F., 1995. Quantal analysis of EPSCs recorded from small numbers of synapses in hippocampal cultures. *Journal of neurophysiology*, 73(3), pp.1145–56.

Berry, M.J. & Meister, M., 1998. Refractoriness and neural precision. *The Journal of neuroscience : the official journal of the Society for Neuroscience*, 18(6), pp.2200–11.

Bezanilla, F., 2005. Voltage-gated ion channels. *IEEE Transactions on Nanobioscience*, 4(1), pp.34–48.

Bialek, W. et al., 1997. Spikes: exploring the neural code. *MIT. Roddey, JC, Girish, B., & Miller, JP (2000). Assessing the performance of neural encoding models in the presence of noise. Journal of Computational Neuroscience*, 8(95), pp.214–221, 267–277.

Borst, a & Theunissen, F., 1999. Information theory and neural coding. *Nat Neurosci*, 2(11), pp.947–957.

Bruce, I.C., 2009. Evaluation of stochastic differential equation approximation of ion channel gating models. *Annals of Biomedical Engineering*, 37(4), pp.824–838.

Calvin, W.H. & Stevens, C.F., 1968. Synaptic noise and other sources of randomness in motoneuron interspike intervals. *Journal of neurophysiology*, 31(August), pp.574–587.

Cang, J. & Isaacson, J.S., 2003. In vivo whole-cell recording of odor-evoked synaptic transmission in the rat olfactory bulb. *The Journal of neuroscience : the official journal of the Society for Neuroscience*, 23(10), pp.4108–16.

Carleton, A., Accolla, R. & Simon, S.A., 2010. Coding In The Mammalian Gustatory System. *Trends in neurosciences*, 33(7), pp.326–334.

Catterall, W.A., 1995. Structure and function of voltage-gated ion channels. *Annual review of biochemistry*, 64, pp.493–531.

Cole, K.S. & Hodgkin, a L., 1939. Membrane and Protoplasm Resistance in the Squid Giant Axon. *The Journal of general physiology*, 22(5), pp.671–687.

Collins, J.J., Chow, C.C. & Imhoff, T.T., 1995. Stochastic resonance without tuning. *Nature*, 376(6537), p.236.

Curtis, H.J. & Cole, K.S., 1938. Transverse Electric Impedance of the Squid Giant Axon. *The Journal of general physiology*, 21(6), pp.757–65.

Davis, G. & Plaisted-Grant, K., 2014. Low endogenous neural noise in autism. *Autism : the international journal of research and practice*, 19(3), pp.351–62.

Debanne, D. et al., 1997. Action-potential propagation gated by an axonal I(A)-like K+ conductance in hippocampus. *Nature*, 389(6648), pp.286–289.

DeFelice, L.J., 1981. Introduction to Membrane Noise. *NY, NY*, pp.232–236.

Devaux, J.J., 2004. KCNQ2 Is a Nodal K+ Channel. *Journal of Neuroscience*, 24(5), pp.1236–1244.

Ehrenstein, G. & Lecar, H., 1972. The mechanism of signal transmission in nerve axons. *Annual review of Biophysics and Bioengineering*, 1(2), pp.347–68.

Fox, R.F. & Lu, Y.N., 1994. Emergent collective behavior in large numbers of globally coupled independently stochastic ion channels. *Physical Review E*, 49(4), pp.3421–3431.

Gautrais, J. & Thorpe, S., 1998. Rate coding versus temporal order coding: A theoretical approach. *BioSystems*, 48(1–3), pp.57–65.

Georgopoulos, A.P., Schwartz, A.B. & Kettner, R.E., 1986. Neuronal population coding of movement direction. *Science (New York, N.Y.)*, 233(4771), pp.1416–1419.

Gilles, W., Michèle, T. & Khashayar, P., 2010. Intrinsic variability of latency to first-spike. *Biological Cybernetics*, 103(1), pp.43–56.

Goldwyn, J.H. et al., 2011. Stochastic differential equation models for ion channel noise in Hodgkin-Huxley neurons. *Physical Review E*, 83(4), p.41908.

Goldwyn, J.H. & Shea-Brown, E., 2011. The what and where of adding channel noise to the Hodgkin-Huxley equations. *PLoS Computational Biology*, 7(11).

Gollisch, T. & Meister, M., 2008. Rapid neural coding in the retina with relative spike latencies. *Science*, 319(5866), pp.1108–1111.

Golomb, D. et al., 1994. On temporal codes and the spatiotemporal response of neurons in the lateral geniculate nucleus. *Journal of neurophysiology*, 72(December), pp.2990–3003.

Graf von Keyserlingk, D. & Schramm, U., 1984. Diameter of axons and thickness of myelin sheaths of the pyramidal tract fibres in the adult human medullary pyramid. *Anatomischer Anzeiger*, 157(2), pp.97–111.

Gulbis, J.M. et al., 2000. Structure of the cytoplasmic beta subunit-T1 assembly of voltage-dependent K+ channels. *Science*, 289(5476), pp.123–7.

Hassard, B., 1978. Bifurcation of periodic solutions of the Hodgkin-Huxley model for the squid giant axon. *Journal of Theoretical Biology*, 71(3), pp.401–420.

Heil, P. et al., 2011. Auditory Cortical Onset Responses Revisited . II . Response Strength Auditory Cortical Onset Responses Revisited . II . Response Strength. , pp.2642–2660.

Helmholtz, H. von, 1885. On the sensations of tone as a physiological basis for the theory of music.

Hille, B., 2001. Ion Channel Excitable Membranes. *Sunderland Massachusetts USA*, pp.1–37.

Hille, B., 1978. Ionic channels in excitable membranes. Current problems and biophysical approaches. *Biophysical journal*, 22(2), pp.283–94.

Hodgkin, A.L. & Huxley, A.F., 1952. A quantitative description of membrane current and its application to conduction and excitation in nerve. *Bulletin of Mathematical Biology*, 52(1–2), pp.25–71.

Hodgkin, A.L. & Huxley, A.F., 1952. The dual effect of membrane potential on sodium conductance in the giant axon of Loligo. *The Journal of Physiology*, 116, pp.497–506.

Hodgkin, A.L., Huxley, A.F. & Katz, B., 1949. Ionic currents underlying activity in the giant axon of the squid. *Archives des Sciences Physiologiques*, 3(2), pp.129–150.

Hodgkin, A.L., Huxley, A.F. & Katz, B., 1951. The effect of sodium ions on the electrical activity of the giant axon of the squid. *The Journal of physiology*, 108(1), pp.37–77.

Hodgkin, A.L. & Rushton, W.A.H., 1946. The electrical constants of a crustacean nerve fibre. *Proceedings of the Royal Society of London B: Biological Sciences*, 133(873), pp.444–479.

Huxley, A.F. & Stämpeli, R., 1949. Evidence for saltatory conduction in peripheral myelinated nerve fibres. *The Journal of Physiology*, 108(3), pp.315–339.

Chomiak, T. & Hu, B., 2009. What is the optimal value of the g-ratio for myelinated fibers in the rat CNS? A theoretical approach. *PloS one*, 4(11), p.e7754.

Isom, L.L. et al., 1992. Primary structure and functional expression of the beta 1 subunit of the rat brain sodium channel. *Science (New York, N.Y.)*, 256(5058), pp.839–842.

Isom, L.L. et al., 1995. Structure and function of the Beta2 subunit of brain sodium channels, a transmembrane glycoprotein with a CAM motif. *Cell*, 83(3), pp.433–442.

Johansson, R.S. & Birznieks, I., 2004. First spikes in ensembles of human tactile afferents code complex spatial fingertip events. *Nature neuroscience*, 7(2), pp.170–177.

Johnson, J.B., 1928. Thermal agitation of electricity in conductors. *Physical Review*, 32(1), pp.97–109.

Johnson Andnelson, D.H. & Kiang, Y.S., 1976. Analysis of Discharges Recorded Simultaneously From Pairs of Auditory Nerve Fibers. *Biophysical Journal*, 16(7), pp.719–734.

Jones, S.W., 2006. Are rate constants constant? *The Journal of physiology*, 571(Pt 3), p.502.

Joris, P.X., 1996. Envelope coding in the lateral superior olive. II. Characteristic delays and comparison with responses in the medial superior olive. *Journal of neurophysiology*, 76(4), pp.2137–56.

Kail, R., 1997. The neural noise hypothesis: Evidence from processing speed in adults with multiple sclerosis. *Aging, Neuropsychology, and Cognition*, 4(3), pp.157–165.

Kazen-Gillespie, K. a et al., 2000. Cloning, localization, and functional expression of sodium channel beta1A subunits. *The Journal of biological chemistry*, 275(2), pp.1079–1088.

Kiang, N.Y.S. & Moxon, E.C., 1972. Physiological considerations in artificial stimulation of the inner ear. *Annals of Otology, Rhinology & Laryngology*, 81(5), pp.714–730.

Kuriscak, E. et al., 2015. Biological context of Hebb learning in artificial neural networks, a review. *Neurocomputing*, 152, pp.27–35.

Kuriscak, E. et al., 2012. The effect of neural noise on spike time precision in a detailed CA3 neuron model. *Computational and Mathematical Methods in Medicine*, 2012.

Kuriscak, E., 2002. Vplyv synaptického, kanálového a termického šumu na prenos signálu a informácie neurónom. Disertační práce. *Fyziologický ústav 1. lékařské fakulty Univerzity Karlovy, Praha*.

Kuriščák, E., Trojan, S. & Wünsch, Z., 2002. Model of spike propagation reliability along the myelinated axon corrupted by axonal intrinsic noise sources. *Physiological Research*, 51(2), pp.205–215.

Lai, H.C. & Jan, L.Y., 2006. The distribution and targeting of neuronal voltage-gated ion channels. *Nature reviews. Neuroscience*, 7(7), pp.548–562.

Lee, C., Rohrer, W.H. & Sparks, D.L., 1988. Population coding of saccadic eye movements by neurons in the superior colliculus. *Nature*, 332(6162), pp.357–60.

Lee, S.-G., Neiman, A. & Kim, S., 1998. Coherence resonance in a Hodgkin-Huxley neuron. *Physical Review E*, 57(3), pp.3292–3297.

Liu, R.C. et al., 2001. Variability and information in a neural code of the cat lateral geniculate nucleus. *Journal of neurophysiology*, 86(6), pp.2789–2806.

Malhotra, J.D. et al., 2000. Sodium channel brta subunits mediate homophilic cell adhesion and recruit ankyrin to points of cell-cell contact. *Journal of Biological Chemistry*, 275(15), pp.11383–11388.

Manwani, a & Koch, C., 1999a. Detecting and estimating signals in noisy cable structures, I: Neuronal Noise Sources. *Neural computation*, 11(8), pp.1831–1873.

Manwani, a & Koch, C., 1999b. Detecting and estimating signals in noisy cable structures, II: Information Theoretical Analysis. *Neural computation*, 11(8), pp.1831–1873.

Maynard, E.M. et al., 1999. Neuronal interactions improve cortical population coding of movement direction. *The Journal of neuroscience : the official journal of the Society for Neuroscience*, 19(18), pp.8083–93.

McCullagh, P., 1984. Generalized linear models. *European Journal of Operational Research*, 16(3), pp.285–292.

Miller, C.A. & Matsuoka, A.J., 1999. Electrically evoked single-fiber action potentials from cat: responses to monopolar, monophasic stimulation. , 130, pp.197–218.

Miller, R.N. & Rinzel, J., 1981. The dependence of impulse propagation speed on firing frequency, dispersion, for the Hodgkin-Huxley model. *Biophysical Journal*, 34(2), pp.227–259.

Morgan, K. et al., 2000. Beta 3: an Additional Auxiliary Subunit of the Voltage-Sensitive Sodium Channel That Modulates Channel Gating With Distinct Kinetics. *Proceedings of the National Academy of Sciences of the United States of America*, 97(5), pp.2308–13.

Mountcastle, V., 1956. Modality And Topographic Properties Of Single Neurons Of Cat's Somatic Sensory Cortex.

Murthy, V.N., Sejnowski, T.J. & Stevens, C.F., 1997. Heterogeneous release properties of visualized individual hippocampal synapses. *Neuron*, 18, pp.599–612.

Nicholls, J.G. et al., 2012. From neuron to brain. In Fifth edition. Sunderland, Mass. : Sinauer Associates, [2001] ©2001, pp. 116–118.

Olshausen, B.A. & Field, D.J., 2004. Sparse coding of sensory inputs. *Current Opinion in Neurobiology*, 14(4), pp.481–487.

Optican, L.M. & Richmond, B.J., 1987. Temporal encoding of two-dimensional patterns by single units in primate inferior temporal cortex. 3. Information Theoretic Analysis. *Journal of Neurophysiology*, 57(1), pp.162–178.

Ozer, M. et al., 2009. Spike latency and jitter of neuronal membrane patches with stochastic Hodgkin-Huxley channels. *Journal of Theoretical Biology*, 261(1), pp.83–92.

Paffi, A. et al., 2015. Restoring the encoding properties of a stochastic neuron model by an exogenous noise. *Frontiers in Computational Neuroscience*, 9(May), pp.1–11.

Palm, G. & Sommer, F.T., 1996. Associative data storage and retrieval in neural networks. In *Models of neural networks III*. Springer, pp. 79–118.

Paré, D. et al., 1998. Impact of spontaneous synaptic activity on the resting properties of cat neocortical pyramidal neurons In vivo. *Journal of neurophysiology*, 79(3), pp.1450–1460.

Parnas, B.R., 1996. Noise and neuronal populations conspire to encode simple waveforms reliably. *IEEE transactions on biomedical engineering*, 43(3), pp.313–318.

Pongs, O. et al., 1999. Functional and molecular aspects of voltage-gated K+ channel β subunits. *Annals of the New York Academy of Sciences*, 868(May), pp.344–355.

Pospischil, M. et al., 2008. Minimal Hodgkin-Huxley type models for different classes of cortical and thalamic neurons. *Biological Cybernetics*, 99(4–5), pp.427–441.

Qin, F., Auerbach, A. & Sachs, F., 2000. A direct optimization approach to hidden Markov modeling for single channel kinetics. *Biophysical Journal*, 79(4), pp.1915–1927.

Qin, F., Auerbach, A. & Sachs, F., 1996. Estimating single-channel kinetic parameters from idealized patch-clamp data containing missed events. *Biophysical journal*, 70(1), pp.264–80.

Qin, N. et al., 2003. Molecular cloning and functional expression of the human sodium channel beta1B subunit, a novel splicing variant of the beta1 subunit. *European Journal of Biochemistry*, 270(23), pp.4762–4770.

Rall, W., 1967. Distinguishing Theoretical Synaptic Potentials Computed For Different Some-dendritic Distributions Of Synaptic Input.

Rhodes, K.J. et al., 1997. Association and colocalization of the Kvbeta1 and Kvbeta2 beta-subunits with Kv1 alpha-subunits in mammalian brain K+ channel complexes. *The Journal of neuroscience : the official journal of the Society for Neuroscience*, 17(21), pp.8246–8258.

Ritchie, J.M. & Rogart, R.B., 1977. Density of sodium channels in mammalian myelinated nerve fibers and nature of the axonal membrane under the myelin sheath. *Proceedings of the National Academy of Sciences of the United States of America*, 74(1), pp.211–215.

Rokem, A., 2005. Spike-Timing Precision Underlies the Coding Efficiency of Auditory Receptor Neurons. *Journal of Neurophysiology*, 95(4), pp.2541–2552.

Ropireddy, D. et al., 2011. Axonal morphometry of hippocampal pyramidal neurons semi-automatically reconstructed after in vivo labeling in different CA3 locations. *Brain Structure and Function*, 216(1), pp.1–15.

Rosenbluth, J., 1976. Intramembranous particle distribution at the node of Ranvier and adjacent axolemma in myelinated axons of the frog brain. *Journal of neurocytology*, 5(6), pp.731–745.

van Rossum, M.C.W., O'Brian, B.J. & Smith, R.G., 2003. Effects of noise on the spike timing precision of retinal ganglion cells. *J. Neurophysiology*, 89, pp.2406–2419.

Rubinstein, J.T. & Miller, C.A., 1999. How do cochlear prostheses work? *Current Opinion in Neurobiology*, 9(4), pp.399–404.

Sanders, F.K., 1948. The Thickness of the Myelin Sheaths of Normal and Regenerating Peripheral Nerve Fibres. *Proceedings of the Royal Society of London. Series B, Biological Sciences*, 135(880), pp.323–357.

Sanders, F.K. & Whitteridge, D., 1946. Conduction velocity and myelin thickness in regenerating nerve fibres. *Journal of Physiology*, 105, pp.152–174.

Sengupta, B., Laughlin, S.B. & Niven, J.E., 2010. Comparison of Langevin and Markov channel noise models for neuronal signal generation. *Physical Review E - Statistical, Nonlinear, and Soft Matter Physics*, 81(1), pp.1–12.

Sewell, B.Y.W.F., 1984. the Relation Between the Endocochlear Potential and. , pp.685–696.

Shadlen, M.N. & Newsome, W.T., 1998. The variable discharge of cortical neurons: implications for connectivity, computation, and information coding. *The Journal of neuroscience : the official journal of the Society for Neuroscience*, 18(10), pp.3870–96.

Shannon, C.E., 1948. A Mathematical Theory of Communication. *Biophysical journal*, 71(1), pp.148–155.

Simmons, D.R. et al., 2009. Vision in autism spectrum disorders. *Vision Research*, 49(22), pp.2705–2739.

Smart, S.L. et al., 1998. Deletion of the K(v)1.1 Potassium Channel Causes Epilepsy in Mice. *Neuron*, 20(4), pp.809–819.

Spanne, A. & Jorntell, H., 2015. Questioning the role of sparse coding in the brain. *Trends in Neurosciences*, 38(7), pp.417–427.

Sperelakis, N., 2012. Cell physiology source book: essentials of membrane biophysics. In Elsevier, pp. 124–145, 325–367.

Stacey, W.C. & Durand, D.M., 2001. Synaptic noise improves detection of subthreshold signals in hippocampal CA1 neurons. *Journal of neurophysiology*, 86, pp.1104–1112.

Stein, R.B., Gossen, E.R. & Jones, K.E., 2005. Neuronal variability: noise or part of the signal? *Nature Reviews Neuroscience*, 6(May), pp.389–397.

Stikov, N. et al., 2015. In vivo histology of the myelin g-ratio with magnetic resonance imaging. *NeuroImage*, 118, pp.397–405.

Strassberg, A.F. & DeFelice, L.J., 1993. Limitations of the Hodgkin-Huxley Formalism: Effects of Single Channel Kinetics on Transmembrane Voltage Dynamics. *Neural Computation*, 5(6), pp.843–855.

Stratford, K.J. et al., 1996. Excitatory synaptic inputs to spiny stellate cells in cat visual cortex. *Nature*, 382, pp.258–261.

Tasaki, I., 1959. Conduction of the nerve impulse. *Handbook of physiology*, 1, pp.75–121.

Tasaki, I., 1955. New Measurements of the Capacity and the Resistance of the Myelin Sheath and the Nodal Membrane of the Isolated Frog Nerve Fiber. *Am J Physiol*, 0(181.3), pp.639–650.

Tortora, G.J. & Derrickson, B.H., 2008. *Principles of anatomy and physiology*, John Wiley & Sons.

Traub, R.D. et al., 1994. A branching dendritic model of a rodent CA3 pyramidal neurone. *The Journal of physiology*, 481 (Pt 1(1994), pp.79–95.

Traynelis, S.F. & Jaramillo, F., 1998. Getting the most out of noise in the central nervous system. *Trends in Neurosciences*, 21(4), pp.137–145.

Tveito, A. et al., 2016. Computing rates of Markov models of voltage-gated ion channels by inverting partial differential equations governing the probability density functions of the conducting and non-conducting states. *Mathematical Biosciences*, 277, pp.126–135.

van Vreeswijk, C. & Sompolinsky, H., 1996. Chaos in Neuronal Networks with Balanced Excitatory and Inhibitory Activity. *Science (New York, N.Y.)*, 274, pp.1724–1726.

Welford, A.T., 1965. Performance, biological mechanisms and age: A theoretical sketch. *Behavior, aging, and the nervous system*, pp.3–20.

West, R.M.E., De Schutter, E. & Wilcox, G.L., 1999. Using evolutionary algorithms to search for control parameters in a nonlinear partial differential equation. In *Evolutionary Algorithms*. Springer, pp. 33–64.

White, J.A., Rubinstein, J.T. & Kay, A.R., 2000. Channel noise in neurons. *Trends in Neurosciences*, 23(3), pp.131–137.

White, J. a et al., 1998. Noise from voltage-gated ion channels may influence neuronal dynamics in the entorhinal cortex. *Journal of neurophysiology*, 80(1), pp.262–269.

Wilkinson, D.J., 2011. *Stochastic modelling for systems biology*, CRC press.

Willshaw, D.J., Buneman, O.P. & Longuet-Higgins, H.C., 1969. Non-holographic associative memory. *Nature*.

Yu, F.H. et al., 2003. Sodium channel beta4, a new disulfide-linked auxiliary subunit with similarity to beta2. *The Journal of neuroscience : the official journal of the Society for Neuroscience*, 23(20), pp.7577–85.

Zador, A., 1998. Impact of synaptic unreliability on the information transmitted by spiking neurons. *Journal of neurophysiology*, 79(3), pp.1219–1229.

Zeng, S., 2005. Spatial distribution and function of ion channels on neural axon. *Dissertation*, (March).

Appendix

The source code of our axonal model of mammalian CA3 neuron

```
% rng('default')
% rng(1) % fixes the noise, so that it is the same on every trial

Nseg =200; % number of all segments, number of Ranvier nodes is Nseg/2
simtime = 100; % duration of simulation [ms]
deltaT=.001; % time step [ms]
t=0:deltaT:simtime;

% Axonal parameters
C_membr = .01;% capacitance of one layer of membrane [farad/m2]
R_axial = 1; % axial resistivity [ohm . m]
ax_diam = 0.000020; % axon diameter without myelin [m]
l_intrnod = 146*ax_diam; % length of an internode [m], from (Tasaki 1959)
and (Kuriscak 2002)
l_nodium = l_intrnod/300; % length of the Ranvier node [m] from (Kuriscak
2002)
No_of_myel = 210; % Number of myelin sheaths, (for axon 20um wide it is 210
layers (Kuriscak 2002))
nodal_RL = 0.005; % membrane leakage resistance in the nodes [ohm.m2]
(Kuriscak 2002)
internodal_RL = .05; % membrane leakage resistance in the internodes
[ohm.m2] (kuriscak 2002) The value of the "leak" conductance assigned by
Hodgkin & Huxley (0.0003 S/cm2)

% Constants of the nodal region
ErNa = 115; ErK = -12; % reversal potential for Na and K channels [mV]
Eleak = 5; % leakage reversal [mV];
Cm = 1; % capacitance of an unmyelinated membrane [1uF/cm2]
gdNa = 3; % conductance of Na channels [S/cm2] (Kuriscak 2002, 2012); 2000
channels/um2 (kuriscak 2002); 1200 channels/um2
gsNa = 15e-12; % conductance of one Na channel; 15pS (Kuriscak 2012)
gdK = 1; % conductance of K channels; 0.260 S/cm2 (Kuriscak 2002, 2012);
200 channels/um2 (Kuriscak 2002);
gsK = 17e-12; % conductance of one K channel; 17pS (Kuriscak 2012)
gL = 1/(nodal_RL/(3.14*ax_diam*l_nodium)); % conductance of the leakage
channels [S]
gNa = gdNa*10000*(3.14*ax_diam*l_nodium); % conductance of all Na channels
in the node [S]; x10000 is converison from [/cm2] to [/m2]
gK = gdK*10000*(3.14*ax_diam*l_nodium); % conductance of all K channels in
the node [S]; x10000 is converison from [/cm2] to [/m2]
Cm = C_membr*3.14*ax_diam*l_nodium; % node capacity [F]
```

```
Ra = R_axial*l_nodium/(3.14*(ax_diam/2)^2); % axial resistance [ohm]

% Internodes
mErNa = 115; mErK = -12; % reversal potential for Na and K channels [mV]
mEleak = 5; % leakage reversal [mV];
mgdNa = 0.0008;  % conductance of Na channels [S/cm2] (kuriscak 2002); 20-
25 channels/um2 [2]
mgdK = 0.0026;%  conductance of K channels (kuriscak 2002)
mgL = 1/((No_of_myel*internodal_RL)/(3.14*ax_diam*l_intrnod)); %conductance
of the leakage channels [S]
mgNa = mgdNa*10000*(3.14*ax_diam*l_intrnod); % conductance of all Na
channels in the internode [S]; x10000 is converison from [/cm2] to [/m2]
mgK = mgdK*10000*(3.14*ax_diam*l_intrnod); % conductance of all K channels
in the internode [S]; x10000 is converison from [/cm2] to [/m2]
mCm = C_membr*3.14*ax_diam*l_intrnod/No_of_myel; % internode capacity [F]
mRa = R_axial*l_intrnod/(3.14*(ax_diam/2)^2); % axial resistance [ohm]

I(1:numel(t),1,1:Nseg) = 0; % no input current
I((22/deltaT):(23/deltaT),1,1) = 24e-9;  % injected current in given time
range and segment [A]

% Ion channels
S_Na = 8; % number of possible states of Na channels
S_K  = 5; % number of possible states of K channels
N_Na=round(gNa/gsNa);mN_Na=round(mgNa/gsNa); % the total amount of Na
channels in nodes and internodes
N_K=round(gK/gsK);mN_K=round(mgK/gsK); % the total amount of K channels in
nodes and internodes

% Array sizes
D=zeros(S_Na,S_Na,Nseg);
F=zeros(S_K,S_K,Nseg);
P_Na=zeros(S_Na,S_Na,Nseg);
P_K=zeros(S_K,S_K,Nseg);
V=zeros(numel(t),1,Nseg); I_m=zeros(numel(t),1,Nseg);
n=zeros(numel(t),1,Nseg); h=zeros(numel(t),1,Nseg);
m=zeros(numel(t),1,Nseg);
N_Na_old(1,1:S_Na,1:Nseg)=0.; % number of Na channels in each state
N_K_old(1,1:S_K,1:Nseg)=0.; % number of K channels in each state
V(1,1,1:Nseg) = 5; % Input voltage [mV]

fractions_Na(1,1:S_Na) = [.32 .000067 .0025 .053066 .54 .08 .0043 .000067]
* N_Na; % An approximate fraction of Na channels in each state in an
unexcited cell
fractions_K(1,1:S_K) = [.011 .086 .283 .403 .217] * N_K; % An approximate
fraction of K channels in each state in an unexcited cell

for i= 1:2:Nseg
N_Na_old(1,1:S_Na,i) = round(fractions_Na(1,1:S_Na));
N_K_old(1,1:S_K,i) = round(fractions_K(1,1:S_K));
end

for i= 2:2:Nseg
fractions_Na(1,1:S_Na) = [.32 .000067 .0025 .053066 .54 .08 .0043 .000067]
* mN_Na;
N_Na_old(1,1:S_Na,i) = round(fractions_Na(1,1:S_Na));
fractions_K(1,1:S_K) = [.011 .086 .283 .403 .217] * mN_K;
N_K_old(1,1:S_K,i) = round(fractions_K(1,1:S_K));
end
```

```
for i=1:numel(t)-1

% Rate constants alpha and beta
alfa_n = (.03*  (17.2-V(i,1,:)) ./ (exp((17.2-V(i,1,:))/5)-1) )* deltaT;
beta_n = (.45*exp((12-V(i,1,:))/40))* deltaT;

alfa_m = (.8* (17.2-V(i,1,:)) ./ (exp((17.2-V(i,1,:))/4)-1) )* deltaT;
beta_m = ((.7*(V(i,1,:)-42.2))./(exp((V(i,1,:)-42.2)/5)-1) )* deltaT ;

alfa_h = (.32*exp((42-V(i,1,:))/18))* deltaT;
beta_h = (10/(1+exp((42-V(i,1,:))/5)))* deltaT;

% Transition matrix (probabilities of changing state) for Na channels
P_Na(2,1,:) = beta_m.^3;
P_Na(3,1,:) = beta_m.^2;
P_Na(4,1,:) = beta_m;
P_Na(5,1,:) = beta_h;
P_Na(6,1,:) = beta_m .* beta_h;
P_Na(7,1,:) = beta_m.^2 .* beta_h;
P_Na(8,1,:) = beta_m.^3 .* beta_h;

P_Na(1,2,:) = alfa_m.^3;
P_Na(3,2,:) = alfa_m;
P_Na(4,2,:) = alfa_m.^2;
P_Na(5,2,:) = alfa_m.^3 .* beta_h;
P_Na(6,2,:) = alfa_m.^2 .* beta_h;
P_Na(7,2,:) = alfa_m .* beta_h;
P_Na(8,2,:) = beta_h;

P_Na(1,3,:) = 3 * alfa_m.^2;
P_Na(2,3,:) = 3 * beta_m;
P_Na(4,3,:) = 2 * alfa_m;
P_Na(5,3,:) = 3 * alfa_m.^2 .* beta_h;
P_Na(6,3,:) = 2 * alfa_m .* beta_h;
P_Na(7,3,:) = beta_h;
P_Na(8,3,:) = 3 * beta_m .* beta_h;

P_Na(1,4,:) = 3 * alfa_m;
P_Na(2,4,:) = 3 * beta_m.^2;
P_Na(3,4,:) = 2 * beta_m;
P_Na(5,4,:) = 3 * alfa_m .* beta_h;
P_Na(6,4,:) = beta_h;
P_Na(7,4,:) = 2 * beta_m .* beta_h;
P_Na(8,4,:) = 3 * beta_m.^2 .* beta_h;

P_Na(1,5,:) = alfa_h;
P_Na(2,5,:) = beta_m.^3 .* alfa_h;
P_Na(3,5,:) = beta_m.^2 .* alfa_h;
P_Na(4,5,:) = beta_m .* alfa_h;
P_Na(6,5,:) = beta_m;
P_Na(7,5,:) = beta_m.^2;
P_Na(8,5,:) = beta_m.^3;

P_Na(1,6,:) = 3 * alfa_m .* alfa_h;
P_Na(2,6,:) = 3 * beta_m.^2 .* alfa_h;
P_Na(3,6,:) = 2 * alfa_m.^2 .* alfa_h;
P_Na(4,6,:) = alfa_h;
```

```
P_Na(5,6,:) = 3 * alfa_m;
P_Na(7,6,:) = 2 * beta_m;
P_Na(8,6,:) = 3 * beta_m.^2;

P_Na(1,7,:) = 3 * alfa_m.^2 .* alfa_h;
P_Na(2,7,:) = 3 * beta_m .* alfa_h;
P_Na(3,7,:) = alfa_h;
P_Na(4,7,:) = 2 * alfa_m .* alfa_h;
P_Na(5,7,:) = 3 * alfa_m.^2;
P_Na(6,7,:) = 2 * alfa_m;
P_Na(8,7,:) = 3 * beta_m;

P_Na(1,8,:) = alfa_m.^3 .* alfa_h;
P_Na(2,8,:) = alfa_h;
P_Na(3,8,:) = alfa_m .* alfa_h;
P_Na(4,8,:) = alfa_m.^2 .* alfa_h;
P_Na(5,8,:) = alfa_m.^3;
P_Na(6,8,:) = alfa_m.^2;
P_Na(7,8,:) = alfa_m;

% Transition matrix (probabilities of changing state) for K channels
P_K(2,1,:) = alfa_n;
P_K(3,1,:) = alfa_n.^2;
P_K(4,1,:) = alfa_n.^3;
P_K(5,1,:) = alfa_n.^4;

P_K(1,2,:) = 4 * beta_n;
P_K(3,2,:) = 2 * alfa_n;
P_K(4,2,:) = 3 * alfa_n.^2;
P_K(5,2,:) = 4 * alfa_n.^3;

P_K(1,3,:) = 6 * beta_n.^2;
P_K(2,3,:) = 3 * beta_n;
P_K(4,3,:) = 3 * alfa_n;
P_K(5,3,:) = 6 * alfa_n.^2;

P_K(1,4,:) = 4 * beta_n.^3;
P_K(2,4,:) = 3 * beta_n.^2;
P_K(3,4,:) = 2 * beta_n;
P_K(5,4,:) = 4 * alfa_n;

P_K(1,5,:) = beta_n.^4;
P_K(2,5,:) = beta_n.^3;
P_K(3,5,:) = beta_n.^2;
P_K(4,5,:) = beta_n;

% A random number D of transitted Na channels from Gaussian distribution
N_Na_old_inv=permute(N_Na_old,[2 1 3]);
D = (sqrt(P_Na .* repmat(N_Na_old_inv,1,S_Na) .* (1-P_Na)) .*
randn(8,8,Nseg)) + (P_Na .* repmat(N_Na_old_inv,1,S_Na));
D(D<0) = 0; D = round(D); % Correction of negative values

Incoming_Na = sum(D,1); % sum of all incoming channels
Outgoing_Na_rows = sum(D,2); % sum of all channels leaving the state
Outgoing_Na = permute(Outgoing_Na_rows,[2 1 3]); % rows to columns
conversion
```

```
N_Na_new = N_Na_old + Incoming_Na - Outgoing_Na; % new amount of channels
in each state
N_Na_old = N_Na_new; % update of the new state

% A random number F of transitted K channels from Gaussian distribution
N_K_old_inv=permute(N_K_old,[2 1 3]);
F = (sqrt(P_K .* repmat(N_K_old_inv,1,S_K) .* (1-P_K)) .* randn(5,5,Nseg))
+ (P_K .* repmat(N_K_old_inv,1,S_K));
F(F<0) = 0; F = round(F); % Correction of negative values

Incoming_K = sum(F,1); % sum of all incoming channels
Outgoing_K_rows = sum(F,2); % sum of all channels leaving the state
Outgoing_K = permute(Outgoing_K_rows,[2 1 3]); % rows to columns conversion

N_K_new = N_K_old + Incoming_K - Outgoing_K; % new amount of channels in
each state
N_K_old = N_K_new; % update of the new state

% Amount of open Na and K channels
nO_Na = N_Na_new(1,S_Na,1:Nseg);
nO_K = N_K_new(1,1,1:Nseg);

% The ratio of open Na and K channels to all channels of each type
f_Na = nO_Na / N_Na;
f_K = nO_K / N_K;

% Calculation of total current in internodes
I_Na = mgNa * f_Na .* (V(i,1,:)-mErNa); % current running through Na
channels
I_K = mgK * f_K .*(V(i,1,:)-mErK); % current running through K channels
I_L = mgL *(V(i,1,:)-mEleak); % leakage current
I_m(i,1,1:Nseg)= I(i,1,1:Nseg) - (I_K + I_Na + I_L)/1000; %total current
[A]

% Calculation of total current in the nodes
I_Na = gNa * f_Na(:,:,1:2:Nseg) .* (V(i,1,1:2:Nseg)-ErNa); % current
running through Na channels
I_K = gK * f_K(:,:,1:2:Nseg) .*(V(i,1,1:2:Nseg)-ErK); % current running
through K channels
I_L = gL *(V(i,1,1:2:Nseg)-Eleak); % leakage current
I_m(i,1,1:2:Nseg)= I(i,1,1:2:Nseg) - (I_K + I_Na + I_L)/1000;  %total
current [A]


% Change of voltage at Ranvier nodes, multiplied by 0.001 to convert I into
[A]
V(i+1,1,2:2:Nseg-1) = V(i,1,2:2:Nseg-1) + deltaT*((.001*(V(i,1,1:2:Nseg-2)-
V(i,1,2:2:Nseg-1))/((mRa+Ra)/2) + .001*(V(i,1,3:2:Nseg)-V(i,1,2:2:Nseg-
1))/((mRa+Ra)/2))+  I_m(i,1,2:2:Nseg-1))/mCm; % internodes

V(i+1,1,3:2:Nseg-1) = V(i,1,3:2:Nseg-1) + deltaT*((.001*(V(i,1,2:2:Nseg-2)-
V(i,1,3:2:Nseg-1))/((mRa+Ra)/2) +  .001*(V(i,1,4:2:Nseg)-V(i,1,3:2:Nseg-
1))/((mRa+Ra)/2))+ I_m(i,1,3:2:Nseg-1))/Cm; % nodes

V(i+1,1,1) = V(i,1,1) + deltaT*(.001*(V(i,1,2)-V(i,1,1))/((mRa+Ra)/2) +
I_m(i,1,1))/Cm; % voltage at first node
```

```
V(i+1,1,Nseg) = V(i,1,Nseg) + deltaT*(.001*(V(i,1,Nseg-1)-
V(i,1,Nseg))/((mRa+Ra)/2) +  I_m(i,1,Nseg))/Cm; % last segment

end

V=V-70; % resting potential into -65 mV

% Plot of voltage change in time
figure
plot(t,V(:,1:2:end)); % plots the nodes only
title('Voltage change in time'), xlabel('Time (ms)'), ylabel('Voltage
(mV)')
legend('Usek 1','Usek 2','Usek 3','Usek 4','Usek 5','Usek 6','Usek 7')
```